Catalytic hydrogenation reaction micro-kinetic model for dibenzyltoluene as liquid organic hydrogen carrier

Aleksandra Tomić [a], Brett Pomeroy [b], Branislav Todić [a], Blaž Likozar [b,*], Nikola Nikačević [a,*]

[a] University of Belgrade, Faculty of Technology and Metallurgy, Karnegijeva 4, 1100 Belgrade, Serbia
[b] Department of Catalysis and Chemical Reaction Engineering, National Institute of Chemistry, Hajdrihova 19, 1000 Ljubljana, Slovenia

HIGHLIGHTS

- Experimental hydrogenation of DBT-based LOHC mixture over Ru/Al$_2$O$_3$ particles.
- Influence of temperature, pressure, stirring, initial LOHC and catalyst amount.
- Micro-kinetic model with Langmuir-Hinshelwood mechanism and dissociative adsorption.
- Parameter estimation using genetic algorithm and Levenberg–Marquardt algorithm.
- Excellent concentration profile trends and parameter influence predictions.

GRAPHICAL ABSTRACT
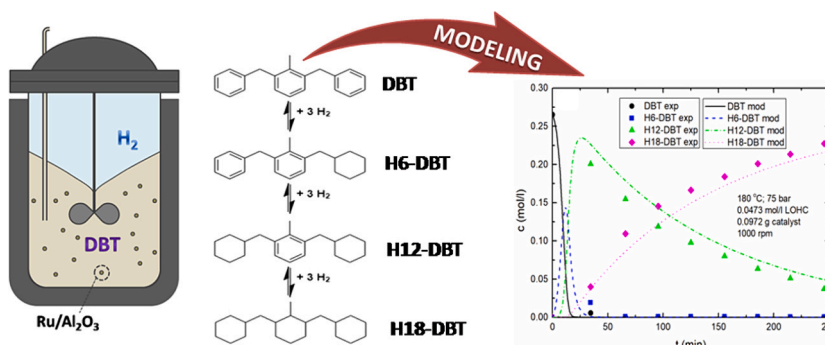
ABSTRACT

The implementation of the liquid organic hydrogen carrier (LOHC) technology for efficient energy storage requires the development of a reliable kinetic model for both hydrogenation and dehydrogenation processes. In this research study, the catalytic hydrocarbon saturation for a dibenzyltoluene (DBT) mixture solution, containing dibenzylbenzene (DBB), dibenzylethylbenzene (DBEB) and impurities has been performed in the presence of Ru/Al$_2$O$_3$ particles. The influence of different reaction conditions, such as temperature, pressure, initial reactant concentration, catalyst amount and stirring speed has been examined. A measurement-based system micro-kinetics, based on the Langmuir–Hinshelwood mechanism with dissociative H$_2$ surface adsorption, has been derived. H$_2$ thermodynamic solubility equilibrium was defined through Henry's law. The adsorbing, desorption and reactivity of inert solvent molecules was not considered to be relevant. The mass transfer resistance over 1000 rpm stirring speed was negligible. Relative- and mean squared error of representation were 40.9% and 1.00×10^{-4}, respectively. Expressions gave an excellent data prediction for the profile period trends with a relatively accurate estimation of H$_2$ intermediates' rate selectivity, H$_2$-covered area approximation and pathway rate-determining steps. Due to the lack of commercially available standard chemical compounds for quantitative analysis techniques, a novel experiment-based numerical calibration method was developed. Mean field (micro) kinetics represent an advancement in the mesoscale mechanistic understanding of physical interface phenomena. This also enables catalysis structure–activity relationships, unlocking the methodology for new LOHC reaching

beyond traditional, such as ammonia, methanol and formate, which do not release H$_2$ alone. Integrated multi-scale simulations could include fluidics later on.

1. Introduction

Global expansion of industrial, transportation and commercial activities in past decades has resulted in a rapid increase in energy consumption. Despite their negative impact on the climate and the environment, fossil-based fuels are still predominantly used to meet these energy requirements [1]. In 2019, the European Commission proposed the European Green Deal, which sets a path for a 55% greenhouse gas (GHG) emission reduction by 2030 and complete climateneutrality by 2050 [2]. The realization of these goals depends on the exploitation of renewable sources, which have been widely explored [3]. However, the fluctuating energy production represents the main issue which imposes a need for reliable storage systems. A possible solution is the use of batteries, but their limitations, such as slow charging, unavailability and negative impact on the environment from exploitation of certain materials, make this option less sustainable. One of the alternatives could be to use electrical energy from renewables to produce a secondary energy carrier, such as green hydrogen gas [4 – 7].

From the environmental standpoint, hydrogen represents an excellent energy source with carbon-free combustion. This gas exhibits great potential for energy storage with a high specific energy of 120 MJ/kg [8,9]. However, approximately 95% of produced hydrogen is immediately used at the production site, due to its unfavorable characteristics related to storage and transportation [10]. Low gas density results in significantly lower volumetric energy density (8 MJ/l), compared to conventional fuels (32 MJ/l for gasoline) [9]. Thus, the use of hydrogen as an energy carrier depends on the efficient storage methods, which enable higher volumetric energy content. The most commonly used options include gas compression (200–700 bar) and liquefaction at cryogenic conditions ($-253°C$). Both processes have high energy requirements, in order to achieve the necessary pressure and temperature. Moreover, boil-off losses in case of liquid hydrogen further reduce the efficiency of this storage method [7,8,11,12]. Hydrogen is also stored in the form of metal hydrides, but its release can be challenging and often requires additional heat [13].
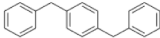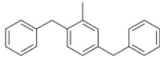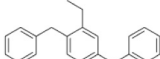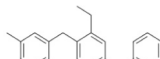
Lately, research has been focused on another storage method – liquid organic hydrogen carriers (LOHC). They represent a group of organic liquids or low melting point solids, with unsaturated covalent double bonds. Hydrogenation of LOHC molecules is an exothermic heterogeneous catalytic process, usually conducted at elevated pressure (10 – 50 bar) and temperature (100 – 250 $°C$), in the presence of Ru-based catalysts [12,14]. This process is reversible, which allows for a hydrogen release at the point of consumption. Endothermic catalytic dehydrogenation is conducted at even higher temperature (150–400 $°C$)

and low pressure (1 – 5 bar), usually over Pt or Pd catalysts [12,14,15]. LOHC should reach high energy density values upon hydrogenation, be liquid in a wide temperature range, have low toxicity and high thermal stability [5,16]. It is important that dehydrogenation temperature does not exceed the boiling point of the selected LOHC, in order for high purity hydrogen to be generated. Since hydrogen release requires elevated temperatures, LOHC manifest negligible hydrogen losses [1,3,14,15].

Oligomers of toluene have shown great hydrogen storage potential and were proposed as the third generation of LOHC [12]. Dibenzyltoluene (DBT) has first been considered as an LOHC by Brückner et al. [17] in 2014. With a storage capacity of 6.2 wt%, low melting ($-34°C$) and high boiling point (390 $°C$), this compound remains one of the most researched LOHC. However, fast hydrogen release requires higher dehydrogenation temperatures, which in return promotes by-product formation and reduces hydrogen purity. Considerable efforts have been made in attempts to resolve this issue by selecting the most efficient catalyst design (usually Pt-based) and optimal dehydrogenation temperature [18–24]. LOHC technology has shown great potential for practical use in fuel cell systems, which has been thoroughly researched [25 – 28]. Significant improvement in hydrogen production was reported by Ali et al. [29] upon continuous dehydrogenation of H18-DBT inside a microchannel reactor.

DBT hydrogenation has also attracted attention, although it has not been as extensively researched as DBT dehydrogenation, which less thermodynamically favorable and can suffer from different issues regarding catalyst deactivation and product purity. In 2016, Do et al. [30] have identified the most probable reaction pathway for hydrogen loading in the presence of Ru/Al$_2$O$_3$ by ^{1}H NMR spectroscopy and HPLC. Detailed spectral analysis confirmed side-ring preference for hydrogenation, with middle-ring hydrogenation as the final reaction step. In their parametric study, Ali et al. [31] have hydrogenated DBT over various catalysts and have found that Raney-Ni showed the highest activity. Other reaction conditions, such as temperature, pressure, stirring speed, Raney-Ni and DBT loading were also varied and their optimal values defined. The same group of authors has expanded this parametric study [32] by examining the influence of temperature on different catalysts' activity. Kim et al. [33] have recommended a Ru/MgO catalyst for fast hydrogenation of toluene oligomers at low temperatures. They concluded that this catalyst promotes both homolytic and heterolytic hydrogen adsorption, which was confirmed by density functional theory calculations. Further research by Kim et al. [34], focused on the K-added Ru/MgO catalyst for hydrogenation of aromatic LOHC at low temperatures and this catalyst expressed maximum activity with 0.02 wt% K.

Table 1
Composition of dibenzyltoluene mixture.

	Compound	Abbreviation	Chemical formula	Structure	Molar mass (g/mol)	Molar fraction (%)
1	1,4-dibenzylbenzene	1,4-DBB	C$_{20}$H$_{18}$		258	∼ 15%
2	dibenzyltoluene	DBT	C$_{21}$H$_{20}$		272	∼ 63%
3	dibenzylethylbenzene	DBEB	C$_{22}$H$_{22}$		286	∼ 19%
4	4-benzyl-2-ethyl-1-(3-methylbenzyl)-benzene	MDBEB	C$_{23}$H$_{24}$		300	∼ 3%

Large-scale application of LOHC technology is highly dependent on the existence of reliable kinetic models for both hydrogenation and dehydrogenation reactions. To the best of the authors' knowledge, kinetic models for DBT hydrogenation have not been reported in present literature. This study presents the first microkinetic model for hydrogenation of a DBT-based mixture in the presence of a Ru/Al$_2$O$_3$ catalyst. An extensive experimental investigation of the hydrogenation reaction was performed, covering a wide range of reaction conditions (temperature, pressure, catalyst loading, initial LOHC concentration and stirring speed). The Langmuir-Hinshelwood mechanism with dissociative hydrogen adsorption was proposed and the microkinetic model was derived from the obtained experimental data. The model parameters were estimated using two optimization methods: genetic algorithm followed by the damped least-squares method (Levenberg–Marquardt algorithm).

2. Experimental

2.1. Materials

For the experimental part of this research, commercially available substances have been used, without additional purification. Commercial dibenzyltoluene mixture (63%, Biosynth AG Rietlistrasse 4, Staad, St. Gallen, Switzerland, reference number FD171211) was selected as the LOHC of interest. Its composition, identified by the GC–MS analysis (described in section 2.4), is presented in Table 1. Note that the structural isomers of these compounds have not been identified and that the structures presented in Table 1 represent arbitrarily selected structural isomers. Since the molar fraction of MDBEB (DBEB with an additional methyl-group, thus MDBEB) in the initial mixture is negligible, this compound has been excluded from further analysis.

Hexane (n-hexane, ≥ 98.5%, Emparta ACS) was chosen as the appropriate solvent and dodecane (n-dodecane, 99.0%, TCI Chemicals) as the internal standard for quantitative sample analysis. Hydrogenation has been performed with commercial hydrogen (5.0, Messer, Bad Soden am Taunas, Germany) in the presence of fine Ru/Al$_2$O$_3$ powder (5 wt% Ru, Sigma Aldrich, St. Louis, MO, USA, reference number 439916; average particle diameter 53 μm), which served as a catalyst. Commercially available nitrogen (5.0, Messer, Bad Soden am Taunas, Germany) was used to purge the reactors prior to the introduction of hydrogen to the system.

2.2. Experimental procedure

The experiments were conducted in batch mode, using a Parr 5000 Multi Reactor System with six parallel reactors (75 ml). This system enables individual pressure and temperature control, while mixing is achieved with a magnetic stirrer (up to 1000 rpm). Temperature and pressure were measured automatically in 30 s intervals. The initial reaction mixture, containing LOHC components and n-hexane, was introduced to the reactor and agitated with a magnetic stirrer. Upon reaching sufficient homogenization, the first sample was collected. Next, the catalyst was introduced to the reaction mixture and the system was then purged with nitrogen (at 50 bar). The system was then pressurized with hydrogen and heating was initiated. Due to safety concerns, all available hydrogen was introduced to the system before heating up and no additional pressurization was performed. Upon reaching the set temperature, the second sample was taken and, from that point, the sampling was conducted every 30 min for 3.5 h. The samples were withdrawn through a dip-tube and filtered with PET filters (CHROMA-FIL Xtra PET, 13 mm, 20 μm) to remove catalyst particles. Quantitative analysis was performed with gas chromatography equipped with a mass spectrophotometer (GC–MS). Prior to analysis, samples were diluted six times with n-hexane, according to literature [35]. The internal standard was added to the initial reaction mixture (1 ml), since dodecane was expected to remain stable throughout the reactions.

Table 2
Experimental conditions.

#	T, °C	p, bar	LOHC : Ru (mol ratio)	N, rpm	V (LOHC), ml	V (hexne), ml
1.	210	75	800	1000	10	30
2.	180	75	800	1000	10	30
3.	150	75	800	1000	10	30
4.	120	75	800	1000	10	30
5.	180	50	800	1000	10	30
6.	210	50	800	1000	10	30
7.	150	50	800	1000	10	30
8.	120	50	800	1000	10	30
9.	180	75	800	1000	15	25
10.	180	75	800	1000	5	35
11.	180	75	1600	1000	10	30
12.	180	75	800	600	10	30
13.	180	75	800	200	10	30
14.	180	75	400	1000	5	35
15.	210	75	800	1000	5	35
16.	210	75	400	1000	5	35
17.	180	100	800	1000	10	30
18.	150	100	800	1000	10	30
19.	180	100	400	1000	10	30

2.3. Experimental conditions

This investigation of DBT-based mixture hydrogenation was performed with 19 experiments at different reaction conditions. Reaction parameters, varied in these experiments, included temperature, pressure, catalyst loading, initial reactant concentration (reactant/solvent ratio) and stirring speed. Pressure and temperature ranges were selected in accordance with the literature, with slight modifications based on the preliminary experimental results [17,36]. The adopted pressure values were significantly higher than those reported in literature, to compensate for the fact that hydrogen could not be continuously supplied. The amount of catalyst was calculated with respect to the initial quantity of LOHC, within the literary recommended range [17,36,37]. After the examination of single reaction parameter influences (# 1–5 and 9–13), simultaneous variation of temperature and pressure was explored (# 6–8). The third set of experiments aimed at best possible hydrogenation from LOHC to their fully hydrogenated forms (# 13–16). Finally, three additional experiments (# 17–19) were performed in attempts to verify model predictions (not used for parameter estimation). Experiment number 2 was selected as a reference (base-case) experiment. Reaction conditions for each of these experiments are presented in Table 2:

As previously mentioned, the temperature in the reactor has been automatically measured every 30 s during the entire reaction. The period between first two samples was the heating-up period (until steady reaction temperature was achieved) for all experiments. In order to simplify the initial temperature profile, the measured temperature values from the heating-up period have been used to form a linear correlation between temperature and reaction time, for different temperature set-points. The parameters of this linear function are given in Table S1 in Supplementary material.

2.4. Quantitative analysis

Samples from the liquid phase have been analyzed using gas chromatography with a mass spectrophotometer (Shimadzu, GCMS-QP2010 Ultra, Kyoto, Japan). Since calibration standards were not commercially available for the chemical species involved in this reaction, GC–MS was not traditionally calibrated. Instead, the response factors for each organic compound present in the system were found numerically. Given the structural similarity of the organic reactants (fully dehydrogenated LOHC), response factors for these compounds were assumed to be equal. A sample of the initial reaction mixture was analyzed, and structural isomers were not detected. Based on the resulting chromatogram, the areas of all peaks for a single fraction, corresponding to all isomers of a
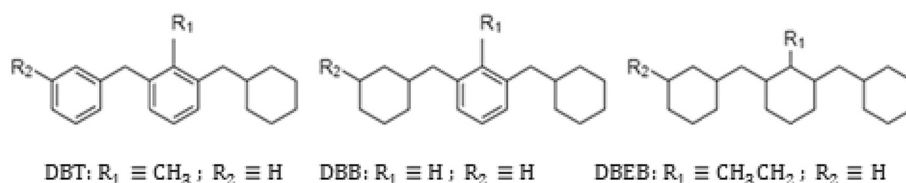
Fig. 1. Intermediates (left – H6-LOHC, middle – H12-LOHC) and final hydrogenation products (right – H18-LOHC).

given compound, were identified. It was then assumed that the ratio of the single fraction area, with respect to the sum of areas for all fractions, is approximately equal to the molar fraction of that fraction (compound) in the initial reaction mixture. The molar fractions were calculated as follows:

$$\frac{A_{r,i}}{\sum_{i=1}^{4} A_{r,i}} = \frac{k_{r,i}\, c_{r,i}}{\sum_{i=1}^{4}\left(k_{r,i}\, c_{r,i}\right)} = \frac{c_{r,i}}{\sum_{i=1}^{4} c_{r,i}} = x_{r,i} \qquad (1)$$

Where $k_{r,i}$ is the response factor of a reactant i and all response factors are equal ($k_{r,1} = k_{r,2} = k_{r,3} = k_{r,4} = k_r$), $A_{r,i}$ is the surface of all peaks of a single fraction, $c_{r,i}$ is the concentration of the fraction, and $x_{r,i}$ is the molar fraction of the reactant i in the initial sample. The next step focused on finding the correction factors for each intermediate and final hydrogenation product (Fig. 1). The process of determining the correction factors for each LOHC compound was based on the structural difference between the two intermediates and the product and is presented in Supplementary Material.

2.5. Catalyst characterization methods

X-ray diffraction (XRD) spectra were achieved using PW3040/60 X'Pert PRO MPD diffractometer at 35 kV and 45 mA with Cu Kα radiation source in the 2θ range from 10° to 80°. The JCPDS database was used for reference. Both hydrogen temperature programmed reduction (H₂-TPR) and carbon monoxide temperature programmed (CO-TPD) were carried out on a Chemisorption Analyzer (AutoChem II, Micrometrics). The catalyst sample (100 mg) was placed inside a quartz U-tube and was initially pretreated in an inert atmosphere (40 mL min⁻¹ of Ar) at 200 °C for 1 h. Following the pretreatment during H₂-TPR, the catalyst was subjected to a flowrate of 40 mL min⁻¹ of 5 vol% H₂ in Ar up to 900 °C with a heating rate of 10 °C/min. A TCD detector calibrated with CuO was implemented to determine hydrogen consumption. During CO-TPD, the catalyst sample was reduced under similar conditions that occurs in situ at the most relevant reaction temperature used for activity tests (210°C for 2 h). Following reduction, catalysts were cooled to −70 °C with liquid N₂, then exposed to 40 mL min⁻¹ of 5 vol% CO in He, purged in pure He, then heated up to 700 °C at a heating rate of 10 °C/min⁻¹ where mass spectrums ($m/z = 28$) were measured by GSD 301 T3 Thermostar Mass Spectrometer. Field-emission scanning electron microscopy (FE-SEM) was conducted to obtain morphological and structural properties of catalyst particles and to determine particle size

distribution. Particle size distribution was estimated by the empirical number-weighted distribution functions and were fitted with a normal distribution function. High-resolution transmission electron microscopy (HR-TEM) analysis was conducted at 200 kV applying a thermionic electron-source.

3. Microkinetic modeling

3.1. Model assumptions

An LOHC mixture for hydrogenation predominantly contains DBT. As described above, besides DBT, this mixture also contained DBEB, DBB and MDBT, all structurally similar to DBT. MDBT has been excluded from modeling, due to its low molar fraction. Catalytic hydrogenation of dibenzyltoluene on Ru/Al₂O₃ particles consists of three reaction stages, which produce stable compounds. In the first stage, dibenzyltoluene undergoes hydrogenation of one side-ring and converts into hexahydro-dibenzyltoluene (H6-DBT). Further hydrogenation of the remaining side ring produces dodecahydro-dibenzyltoluene (H12-DBT). This intermediate reacts to form the final hydrogenation product, perhydro-dibenzyltoluene(H18-DBT), through middle-ring hydrogenation which is considered to be the last reaction step due to steric hindrance caused by the presence of two side-rings [30]. For the selected experimental conditions, it is reasonable to assume that hydrogenation of DBT will be an irreversible process since dehydrogenation occurs at higher temperatures and significantly lower pressure [38]. Fig. 2 presents the most probable reaction pathway for this reaction [30]. As noted above, during the samples analysis, structural isomers have not been identified, thus Fig. 2 presents an arbitrarily selected isomer of DBT and its hydrogenation products.

Because of their structural similarity to DBT, the reaction pathways for DBB and DBEB are considered analogous to the one presented for DBT.

After initial analysis, the following assumptions were used for the kinetic model:

1. Hydrogenation is a heterogeneous catalytic process which occurs only on catalyst surface
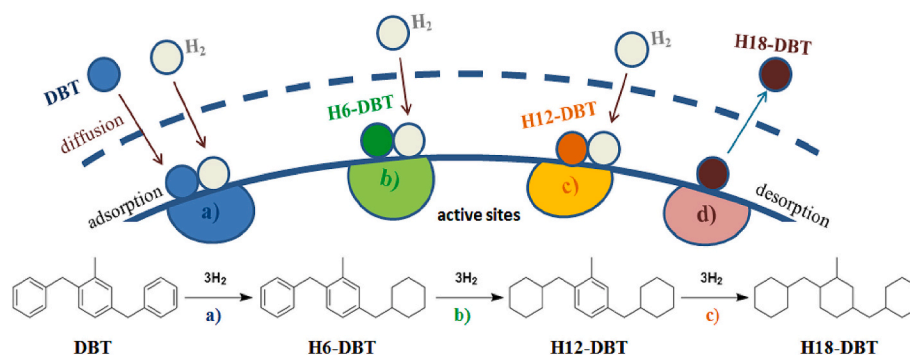2. All active sites on catalyst surface are identical and evenly distributed

Fig. 2. Most probable reaction pathway for DBT hydrogenation with hydrogen and reactant diffusion and adsorption on catalyst active sites [30].

Table 3
DBT hydrogenation mechanism.

DBT adsorption	$DBT + S \overset{K_1}{\leftrightarrow} DBT - S$	(2)
H_2 adsorption	$H_2 + 2S \overset{K_2}{\leftrightarrow} 2H - S$	(3)
DBT to H6-DBT hydrogenation	$DBT - S + H - S \overset{k_3}{\rightarrow} H - DBT - S + S$ $H - DBT - S + H - S \overset{K_4}{\leftrightarrow} H_2 - DBT - S + S$ $H_2 - DBT - S + H - S \overset{K_5}{\leftrightarrow} H_3 - DBT - S + S$ $H_3 - DBT - S + H - S \overset{K_6}{\leftrightarrow} H_4 - DBT - S + S$ $H_4 - DBT - S + H - S \overset{K_7}{\leftrightarrow} H_5 - DBT - S + S$ $H_5 - DBT - S + H - S \overset{K_8}{\leftrightarrow} H_6 - DBT - S + S$ $H_6 - DBT - S \overset{K_9}{\leftrightarrow} H_6 - DBT + S$	(4) (5) (6) (7) (8) (9) (10)
H6-DBT to H12-DBT hydrogenation	$H_6 - DBT + H - S \overset{k_{10}}{\rightarrow} H_7 - DBT - S + S$ $H_7 - DBT - S + H - S \overset{K_{11}}{\leftrightarrow} H_8 - DBT - S + S$ $H_8 - DBT - S + H - S \overset{K_{12}}{\leftrightarrow} H_9 - DBT - S + S$ $H_9 - DBT - S + H - S \overset{K_{13}}{\leftrightarrow} H_{10} - DBT - S + S$ $H_{10} - DBT - S + H - S \overset{K_{14}}{\leftrightarrow} H_{11} - DBT - S + S$ $H_{11} - DBT - S + H - S \overset{K_{15}}{\leftrightarrow} H_{12} - DBT - S + S$ $H_{12} - DBT - S \overset{K_{16}}{\leftrightarrow} H_{12} - DBT + S$	(11) (12) (13) (14) (15) (16) (17)
H12-DBT to H18-DBT hydrogenation	$H_{12} - DBT + H - S \overset{k_{17}}{\rightarrow} H_{13} - DBT - S + S$ $H_{13} - DBT - S + H - S \overset{K_{18}}{\leftrightarrow} H_{14} - DBT - S + S$ $H_{14} - DBT - S + H - S \overset{K_{19}}{\leftrightarrow} H_{15} - DBT - S + S$ $H_{15} - DBT - S + H - S \overset{K_{20}}{\leftrightarrow} H_{16} - DBT - S + S$ $H_{16} - DBT - S + H - S \overset{K_{21}}{\leftrightarrow} H_{17} - DBT - S + S$ $H_{17} - DBT - S + H - S \overset{K_{22}}{\leftrightarrow} H_{18} - DBT - S + S$ $H_{18} - DBT - S \overset{K_{23}}{\leftrightarrow} H_{18} - DBT + S$	(18) (19) (20) (21) (22) (23) (24)

3. Hydrogen solubility has been defined based on the solubility in pure n-hexane (Henry's law)
4. Ideal gas law has been used for hydrogen in the gaseous phase
5. Mass transfer resistance between gaseous and liquid phase is considered negligible due to sufficient mixing
6. Internal (diffusional) mass transfer resistance in particles has been neglected (due to small catalyst particles)
7. All reactants and their hydrogenation products have the same adsorption equilibrium constant

8. Adsorption and desorption of solvent molecules are not considered (assumed negligible)
9. Adsorption and desorption processes are not temperature dependent
10. Decomposition of LOHC and their hydrogenation products is not occurring *(possibly not accurate for H18-DBB)*
11. Reaction rate constants follow the Arrhenius law

Reaction mechanism has been defined using the Langmuir-Hinshelwood approach, with dissociative adsorption of hydrogen. Partial reaction order with respect to hydrogen was assumed to be $p = 1$, based on preliminary parameter estimation. Based on the experimental results for stirring speed variations and literature reports [31], external mass transfer limitations have been considered negligible (see section 4.3). As for the internal mass transfer, it has been assumed that this process had negligible influence on overall LOHC hydrogenation due to the small Ru/Al$_2$O$_3$ particles used in these experiments (average $d_p = 53\ \mu m$) [39]. This was also confirmed by calculating the Weisz-Prater criterion (N_{WP}) for hydrogen and DBT, which were 0.13 and 0.028, respectively (see Supplementary material). Since the criterion is defined as $N_{WP} \leq 0.3$, the assumption of negligible mass transfer resistance in catalyst pores was verified. Temperature influence on adsorption/desorption rates was determined to be minimal, since the introduction of temperature dependence of equilibrium constants had very little effect on the fit quality.

3.2. Reaction mechanism and model setup

3.2.1. Langmuir-Hinshelwood mechanism with dissociative adsorption of H_2

This reaction mechanism includes dissociative adsorption of hydrogen on the catalyst surface, as shown in Eq. (3), where *S* indicates the free active site. It is assumed that the rate determining step for single ring hydrogenation is addition of the first hydrogen atom, which breaks the stable benzene ring structure, as supported by literature [40]. The following equations, given in Table 3, represent the hydrogenation mechanism for DBT hydrogenation.

As previously mentioned, due to the structural similarity, hydrogenation mechanism for DBB and DBEB are analogous to that of DBT. Therefore, reaction steps defined in Eqs. (2–24) are the same (DBB and DBEB replacing DBT) and are presented in Supplementary material.

Additionally, this mechanism assumes that adsorption/desorption processes have achieved equilibrium and these steps are defined by equilibrium constants $K_1 - K_{23}$ for DBT, $K_1' - K_{23}'$ for DBB, and $K_1'' - K_{23}''$ for DBEB. Based on the rate determining steps for DBT (Eqs. (4), (11) and (18)), the following reaction rates are defined as:

$$r_1 = k_3[DBT - S][H - S]^p \qquad (25)$$

$$r_2 = k_{10}[H6 - DBT - S][H - S]^p \qquad (26)$$

$$r_3 = k_{17}[H12 - DBT - S][H - S]^p \qquad (27)$$

where r_1 is the reaction rate of DBT conversion to H6-DBT, r_2 is the rate of H6-DBT to H12-DBT conversion, r_3 is the rate of H18-DBT production from H12-DBT. Reaction rates for rate determining steps in DBB and DBEB hydrogenation are analogous to the ones derived for DBT and are presented in Supplementary material. According to the adsorption equilibrium constants, the following expressions, given in Table 4, can

Table 4
Adsorption equilibrium constants

Constant expression	Concentration of adsorbed species	#
$K_1 = \dfrac{[DBT-S]}{C_{DBT}\,[S]}$	$[DBT-S] = K_1 C_{DBT}\,[S]$	(28)
$K_2 = \dfrac{[H-S]^2}{C_{H_2}[S]^2}$	$[H-S] = \sqrt{K_2 C_{H_2}}\,[S]$	(29)
$\dfrac{1}{K_9} = \dfrac{[H6-DBT-S]}{C_{H6-DBT}\,[S]}$	$[H6-DBT-S] = \dfrac{1}{K_9}C_{H6-DBT}\,[S]$	(30)
$\dfrac{1}{K_{16}} = \dfrac{[H12-DBT-S]}{C_{H12-DBT}\,[S]}$	$[H12-DBT-S] = \dfrac{1}{K_{16}}C_{H12-DBT}\,[S]$	(31)
$\dfrac{1}{K_{23}} = \dfrac{[H18-DBT-S]}{C_{H18-DBT}\,[S]}$	$[H18-DBT-S] = \dfrac{1}{K_{23}}C_{H18-DBT}\,[S]$	(32)
$K_1' = \dfrac{[DBB-S]}{C_{DBB}\,[S]}$	$[DBB-S] = K_1' C_{DBB}\,[S]$	(33)
$\dfrac{1}{K_9'} = \dfrac{[H6-DBB-S]}{C_{H6-DBB}\,[S]}$	$[H6-DBB-S] = \dfrac{1}{K_9'}C_{H6-DBB}\,[S]$	(34)
$\dfrac{1}{K_{16}'} = \dfrac{[H12-DBB-S]}{C_{H12-DBB}\,[S]}$	$[H12-DBB-S] = \dfrac{1}{K_{16}'}C_{H12-DBB}\,[S]$	(35)
$\dfrac{1}{K_{23}'} = \dfrac{[H18-DBB-S]}{C_{H18-DBB}\,[S]}$	$[H18-DBB-S] = \dfrac{1}{K_{23}'}C_{H18-DBB}\,[S]$	(36)
$K_1' = \dfrac{[DBEB-S]}{C_{DBEB}\,[S]}$	$[DBEB-S] = K_1' C_{DBB}\,[S]$	(37)
$\dfrac{1}{K_9'} = \dfrac{[H6-DBEB-S]}{C_{H6-DBEB}\,[S]}$	$[H6-DBEB-S] = \dfrac{1}{K_9'}C_{H6-DBEB}\,[S]$	(38)
$\dfrac{1}{K_{16}'} = \dfrac{[H12-DBEB-S]}{C_{H12-DBEB}\,[S]}$	$[H12-DBEB-S] = \dfrac{1}{K_{16}'}C_{H12-DBEB}\,[S]$	(39)
$\dfrac{1}{K_{23}'} = \dfrac{[H18-DBEB-S]}{C_{H18-DBEB}\,[S]}$	$[H18-DBEB-S] = \dfrac{1}{K_{23}'}C_{H18-DBEB}\,[S]$	(40)

be derived.

Where $[S]$ is the concentration of free active spaces. Based on the Eqs. (28–32), the reaction rates for rate determining steps of DBT hydrogenation can be written as:

$$r_1 = k_3 K_1 C_{DBT}\left(\sqrt{K_2 C_{H_2}}\right)^p [S]^{p+1} \tag{41}$$

$$r_2 = k_{10}\frac{1}{K_9}C_{H6-DBT}\left(\sqrt{K_2 C_{H_2}}\right)^p [S]^{p+1} \tag{42}$$

$$r_3 = k_{17}\frac{1}{K_{16}}C_{H12-DBT}\left(\sqrt{K_2 C_{H_2}}\right)^p [S]^{p+1} \tag{43}$$

The concentration of free active sites ($[S]$) can be determined based on the total active sites balance (44) and expressions (28–40) as follows:

$$
\begin{aligned}
&[S] + [H-S] + [DBT-S] + [H6-DBT-S] + [H12-DBT-S] \\
&\quad + [H18-DBT-S] + [DBB-S] + [H6-DBB-S] + [H12 \\
&\quad - DBB-S] + [H18-DBB-S] + [DBEB-S] + [H6-DBEB-S] \\
&\quad + [H12-DBEB-S] + [H18-DBEB-S] = 1
\end{aligned}
\tag{44}
$$

Since the experiments have been conducted in three-phase batch reactors, the following differential equations represent material balances for DBT, its hydrogenation products and hydrogen:

$$\frac{dC_{DBT}}{dt} = -\frac{\varepsilon}{1-\varepsilon}r_1 \tag{46}$$

$$\frac{dC_{H6-DBT}}{dt} = \frac{\varepsilon}{1-\varepsilon}(r_1 - r_2) \tag{47}$$

$$\frac{dC_{H12-DBT}}{dt} = \frac{\varepsilon}{1-\varepsilon}(r_2 - r_3) \tag{48}$$

$$\frac{dC_{H18-DBT}}{dt} = \frac{\varepsilon}{1-\varepsilon}r_3 \tag{49}$$

$$\frac{1}{V}\frac{dn_{H_2}}{dt} = -\frac{3\varepsilon}{1-\varepsilon}\left(r_1 + r_2 + r_3 + r_1' + r_2' + r_3' + r_1'' + r_2'' + r_3''\right) \tag{50}$$

where n_{H_2} represents the molar amount of hydrogen in the gaseous phase and ε represents the volumetric fraction of the catalyst in the liquid phase volume. The analogous material balances are derived for DBB and DBEB and are presented in the Supplementary material.

The relationship between n_{H_2} and total pressure has been described using ideal gas law:

$$p_g\,V_g = n_{H_2}RT \tag{51}$$

where p_g is the total pressure (approximately equal to the partial pressure of hydrogen), V_g the volume occupied by hydrogen, T absolute temperature and R is the ideal gas constant.

Henry's law has been used to describe the relationship between partial hydrogen pressure and its molar fraction:

$$x_{H_2,eq} = \frac{p_{H_2}\,(bar)}{H_{e_{hexane}}\,(bar)} \tag{52}$$

where Henry's constant for n-hexane was determined from [41]:

$$ln\left(H_{e_{hexane}}\,(atm)\right) = 30.841476 - \frac{814.371094}{T(K)} - 3.709661\,lnT(K) \tag{53}$$

The concentration of dissolved hydrogen is then calculated using the molar fraction of hydrogen and the total concentration:

$$C_{H_2} = x_{H_2,eq}C_{total} \tag{54}$$

The total concentration is calculated as the sum of all components present in the liquid phase, as follows:

$$C_{total} = \sum_{i=1}^{N} C_i \tag{55}$$

where i represents each individual compound (DBT, DBB, DBEB, their hydrogenation products and solvent) and N is the total number of components.

The yield of different hydrogenation products was used in result analysis and calculated with the following expression:

$$Y_i = \frac{C_{Hx-LOHC}}{C_{o_{LOHC}}} * 100\% \tag{56}$$

$$[S] = \cfrac{1}{1 + \sqrt{K_2 C_{H_2}} + K_1 C_{DBT} + \frac{1}{K_9}C_{H6-DBT} + \frac{1}{K_{16}}C_{H12-DBT} + \frac{1}{K_{23}}C_{H18-DBT} + K_1' C_{DBB} + \frac{1}{K_9'}C_{H6-DBB} + \frac{1}{K_{16}'}C_{H12-DBB} + \frac{1}{K_{23}'}C_{H18-DBB} + K_1' C_{DBEB} + \frac{1}{K_9'}C_{H6-DBEB} + \frac{1}{K_{16}'}C_{H12-DBEB} + \frac{1}{K_{23}'}C_{H18-DBEB}} \tag{45}$$

Where $C_{Hx-LOHC}$ is the concentration of the said hydrogenation product and $C_{o_{LOHC}}$ is the initial concentration of the corresponding LOHC.

3.2.2. Experiments for modeling and optimization parameters

The reaction conditions in experiments used for parameter estimation are listed in Table 2 (# 1–11 and 14–16). The experiments with different stirring speed were used to explore the influence of external
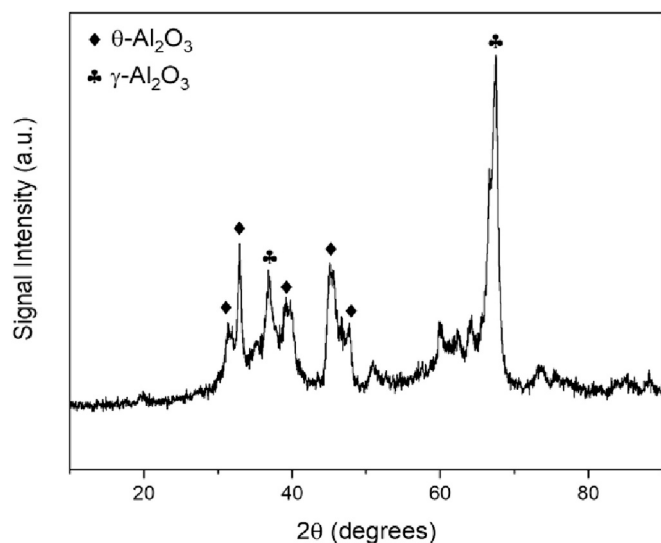
Fig. 3. XRD spectra of the 5%Ru/Al$_2$O$_3$ catalyst.

Fig. 4. H$_2$-TPR profile of the Ru/ Al$_2$O$_3$ catalyst.

mass transfer (see section 4.3) and these experiments have not been used for parameter estimation. Additionally, three experiments at 100 *bar* were used to verify the quality of model predictions (section 4.9).

The Arrhenius parameters for the constants of the rate determining steps have been estimated. Given the assumption of similar adsorption equilibrium for all organic molecules, four constants have been estimated: three for all organic species (DBT, DBB and DBEB and their corresponding products) and one for hydrogen. Therefore, the equilibrium constants for DBT-species presented in Eqs. (28) and (30−32) are reduced to:

$$K_1 = \frac{1}{K_9} = \frac{1}{K_{16}} = \frac{1}{K_{23}} \tag{57}$$

Equilibrium constants for DBB, DBEB and their products were defined analogously.

In total, the number of parameters per hydrogenation reaction of an initial reactant (i.e. DBT) was six kinetic parameters for three reaction steps and two equilibrium constants for reactant and hydrogen adsorption. Parameter estimation was based on the 17 experiments (see Table 2), each with around 100 experimental points (for each reactant, intermediate and final product at different times).

3.2.3. Fitness function and optimization properties

The optimization has been conducted using MatlabR2021a software. The system of differential Eqs. (46–50) and the analogous equations for DBB and DBEB species was solved using *ode15s* for highly non-linear differential equations. The initial conditions included initial DBT, DBB, DBEB concentrations and the initial hydrogen amount (derived from initial partial pressure using ideal gas law), while the concentrations of all hydrogenation products were zero. Two different optimization algorithms have been used to determine the optimal values of the parameters: genetic algorithm (*ga*), followed by the damped least-squares method (*lsqnonlin*). Detailed optimization settings are given in Supplementary Material.

The same objective function was used for both optimization algorithms, defined as:

$$F_{obj} = \frac{1}{M}\sum_{i=1}^{M}\frac{1}{N}\sum_{j=1}^{N}\frac{\left(C_{ij,exp} - C_{ij,mod}\right)^2}{C_{ij,exp}^2} \tag{58}$$

Where M is the number of experiments and N is the number of samples for a given experiment. To avoid division by zero, the experimental points with $C_{ij,exp} = 0$ have been excluded from the calculation.

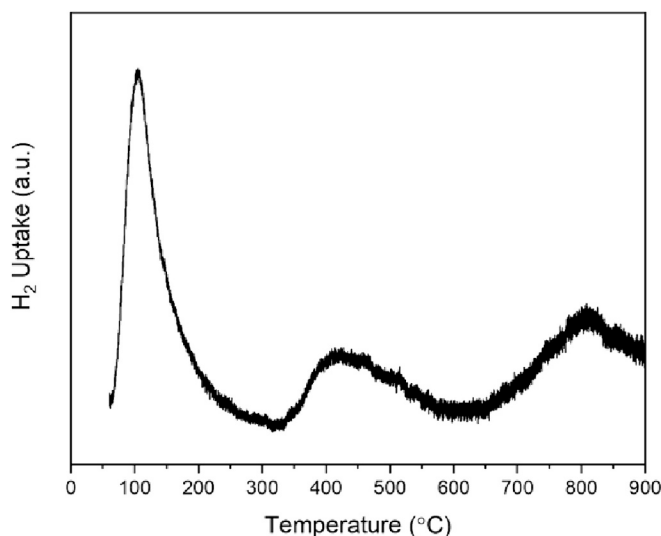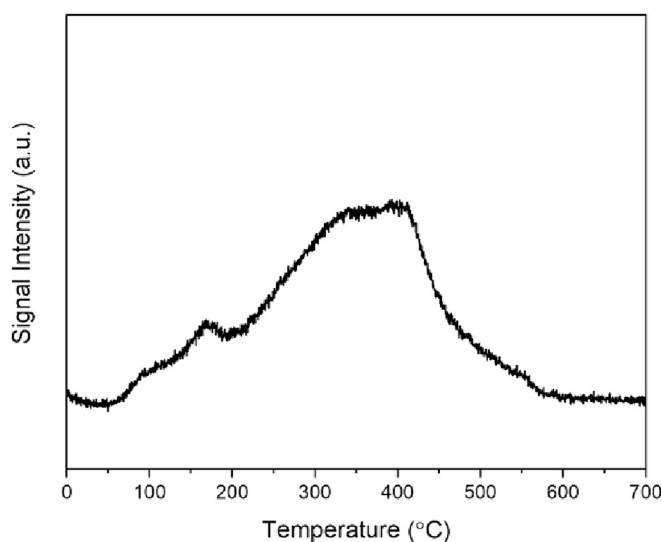Since initial guesses for parameter values could not have been made

Fig. 5. CO-TPD-MS profile ($m/z = 28$) of 5%Ru on alumina catalyst.

with enough certainty, optimization started with a broad search. The search domain for all estimated pre-exponential factors was $1 - 10^{18} l\,mol^{-1}min^{-1}$ and $1 - 10^5 kJ\,mol^{-1}$ for all activation energies. The domain for all equilibrium constants was $10^{-7} - 10^9 l\,mol^{-1}$. These preliminary estimations also provided information with respect to the optimum sensitivity to different initial guesses for model parameters. Another varied parameter in the initial optimizations was the partial reaction order with respect to hydrogen and based on the results, the best fit was obtained with $p = 1$. This partial order has been adopted for all consequent modeling.

Parameter estimation procedure started with the estimation of kinetic and equilibrium constants for experiments at different temperatures and reference initial pressure of 75 *bar*. Based on the obtained kinetic constants for each temperature, pre-exponential factors and activation energies were obtained using the Arrhenius equation. The obtained parameter values were then used as the initial values for estimation based on the experiments at different temperatures and different pressures (experiments # 6–8). After this estimation, the experiments with varied amount of catalyst and initial LOHC concentration (LOHC: solvent ratio) were included and the parameters were estimated simul-
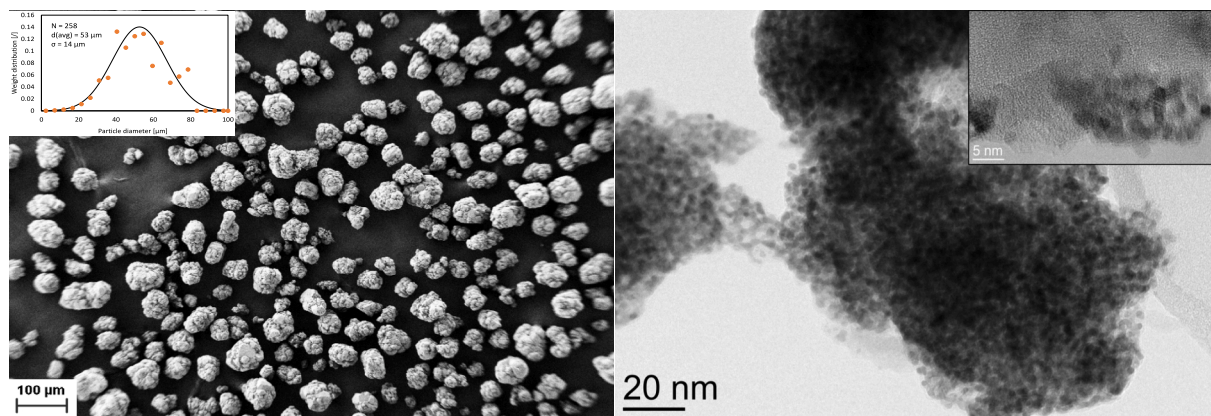
Fig. 6. SEM image of fresh 5wt.%Ru/Al$_2$O$_3$ (left) where the inset is the calculated particle size distribution. TEM images (right) of the catalyst where the inset image at a higher magnification shows the distinct Ru particles.

Table 5
Optimal parameter values.

	Parameter		Units	Value
1.	Pre-exponential factor for k_3	A_3	$\frac{l}{mol\ min}$	$3.92*10^8$
2.	Activation energy for k_3	Ea_3	$\frac{kJ}{mol}$	24.23
3.	Pre-exponential factor for k_{10}	A_{10}	$\frac{l}{mol\ min}$	$2.15*10^8$
4.	Activation energy for k_{10}	Ea_{10}	$\frac{kJ}{mol}$	25.33
5.	Pre-exponential factor for k_{17}	A_{17}	$\frac{l}{mol\ min}$	$1.57*10^5$
6.	Activation energy for k_{17}	Ea_{17}	$\frac{kJ}{mol}$	19.65
7.	Pre-exponential factor for k'_3	A'_3	$\frac{l}{mol\ min}$	$1.22*10^{13}$
8.	Activation energy for k'_3	Ea'_3	$\frac{kJ}{mol}$	28.83
9.	Pre-exponential factor for k'_{10}	A'_{10}	$\frac{l}{mol\ min}$	$1.73*10^8$
10.	Activation energy for k'_{10}	Ea'_{10}	$\frac{kJ}{mol}$	25.46
11.	Pre-exponential factor for k'_{17}	A'_{17}	$\frac{l}{mol\ min}$	$1.10*10^{11}$
12.	Activation energy for k'_{17}	Ea'_{17}	$\frac{kJ}{mol}$	59.21
13.	Pre-exponential factor for k''_3	A''_3	$\frac{l}{mol\ min}$	$4.53*10^7$
14.	Activation energy for k''_3	Ea''_3	$\frac{kJ}{mol}$	21.79
15.	Pre-exponential factor for k''_{10}	A''_{10}	$\frac{l}{mol\ min}$	$1.91*10^8$
16.	Activation energy for k''_{10}	Ea''_{10}	$\frac{kJ}{mol}$	32.01
17.	Pre-exponential factor for k''_{17}	A''_{17}	$\frac{l}{mol\ min}$	$1.41*10^6$
18.	Activation energy for k''_{17}	Ea''_{17}	$\frac{kJ}{mol}$	19.19
19.	Equilibrium constant for HX-DBT	K_1	$\frac{l}{mol}$	$1.19*10^7$
20.	Equilibrium constant for hydrogen	K_2	$\frac{l}{mol}$	$7.64*10^5$
21.	Equilibrium constant for HX-DBB	K'_1	$\frac{l}{mol}$	$3.08*10^7$
22.	Equilibrium constant for HX-DBEB	K'_1	$\frac{l}{mol}$	$1.67*10^7$

taneously for all experimental conditions, with previously obtained values as the initial guesses. The obtained optimum can be considered global with great certainty because of the initial broad domain search and the use of genetic algorithm as the primary optimization method. This algorithm has the ability to expand the domain search even upon reaching a local optimum, as opposed to the traditional gradient-based optimization algorithms.

4. Results and discussion

4.1. Catalyst characterization

Fig. 3 depicts the XRD spectra of the Ru-based catalyst. Peaks associated with both θ (JCPDS #11–0517) and γ-alumina phases (JCPDS #29–63) were present [42,43]. No Ru peaks were observed in the XRD analysis, likely due to Ru$_2$O being below the XRD detection limit (<4 nm) [44]. The TPR profile for the 5 wt% Ru/ Al$_2$O$_3$ catalyst is displayed in Fig. 4 which indicates 3 major peaks centered around 107 °C, 417 °C and 804 °C. The first peak is likely associated with highly dispersed RuO$_2$, the second peak related to bulk RuO$_2$, whereas the third peak is related with RuO$_2$ particles that had a strong interaction with the alumina support [45,46]. Based on the reduction profile of this specific catalyst, it is expected that only the highly dispersed RuO$_2$ particles were readily reduced in situ since the reaction temperature never exceeded 210°C. The resulting CO-TPD-MS spectra ($m/z = 28$ with deduction from CO$_2$ contribution) is shown in Fig. 5, and displays a broad profile between approximately 100 °C up to 600 °C. The estimated number of metallic sites was determined to be 111 μmol/g. SEM image of the 5 wt% Ru/Al$_2$O$_3$ catalyst, presented in Fig. 6 (left), indicates that the average particle diameter of the catalyst particles was 53 μm. Furthermore, it can clearly be seen in the TEM image Fig. 6 (right) that the individual Ru particles are all generally below 5 nm.

4.2. Model parameters

Parameter estimation resulted in optimal values, presented in Table 5. Total relative mean error (RME) for all organic species was 41.49%, while RME for DBT, DBB and DBEB were 40.93%, 47.28% and 38.5%, respectively. This fit gave a mean squared error (MSE) of $1.00 \bullet 10^{-4}$. MSE for DBT, DBB and DBEB were $2.48 \bullet 10^{-4}$, $2.28 \bullet 10^{-5}$ and $1.29 \bullet 10^{-5}$, respectively.

In regards to fit quality, it is important to point out that the deviation of the fit for the lowest concentrations partially accounts for the high relative errors. Moreover, the initial reactant mixture contained three different reacting species, whose hydrogenation reactions were modeled simultaneously. Lastly, the lack of commercially available standards was another issue which could have decreased the reliability of experimental data. Having all of this in mind, the model still gave good predictions, especially with regards to the experimentally obtained qualitative trends.

4.3. Influence of stirring speed and mass transfer

Influence of the possible external mass transfer has been explored through three experiments (# 2, 12 and 13 in Table 2), with different
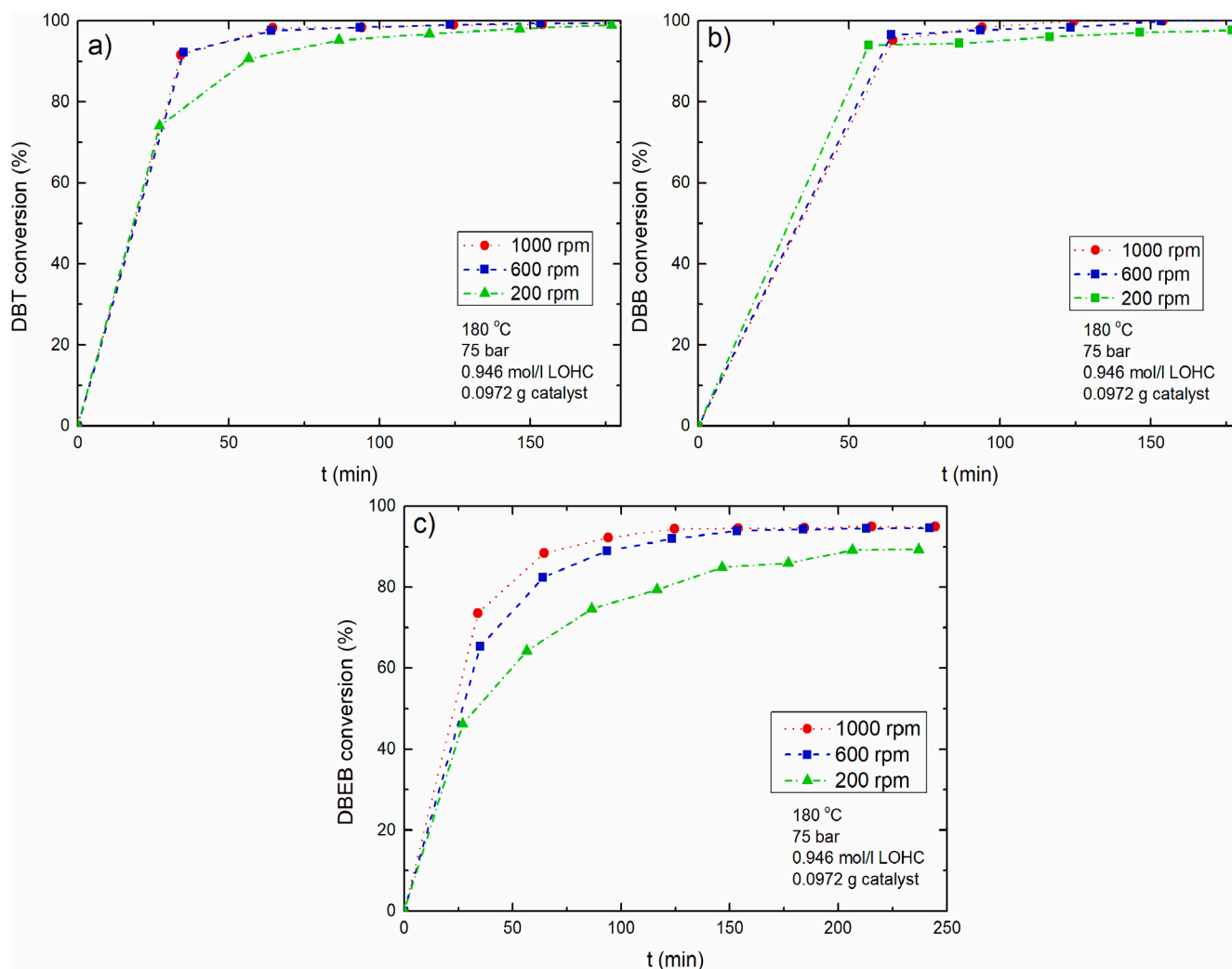
Fig. 7. Influence of stirrer speed on: a) DBT conversion b) DBB conversion c) DBEB conversion.

stirring speeds. The experimental results for DBT, DBB and DBEB conversion for these conditions are presented in Fig. 7. It can be observed that the lowest conversion for all three initial reactants is obtained with 200 *rpm*, which confirms the existence of mass transfer resistance. The increase of stirring speed to 600 *rpm* significantly increased DBT and DBEB conversion. Stirring speed of 1000 *rpm* resulted in slight increase in DBEB conversion in the first two hours of the reaction and no noticeable influence on either DBT or DBB conversion. The slightly higher initial conversion rate for DBB at 200 rpm compared to higher stirring speeds could be contributed to the experimental imprecision and the fact that initial conversion rate for this fast-reacting compound would require more experimental points within the first 60 min of hydrogenation. The obtained results verify that the highest stirrer speed enables fast external mass transfer, compared to the reaction rates of hydrogenation. Furthermore, the difference of DBEB conversion between experiments with 600 and 1000 *rpm* stirring speed could be the result of experimental imprecision. Ali et al. [31] had investigated the influence of stirrer speed on DBT hydrogenation in the presence of Raney-Ni catalyst, at 170°*C* and 0.8 *MPa*. The implemented four stirring speeds, ranging from 200 to 1100 *rpm*, had little effect on hydrogen uptake over the course of 10 *h*. Based on experimental findings in this study, as well as the literature reports, it was concluded that external mass transfer can be neglected above 1000 *rpm*. Calculation of the Weisz-Prater criteria for hydrogen and DBT (see model assumptions in section 3.1 and Supplementary Material) has confirmed that internal

mass transfer can also be neglected. Therefore, the obtained kinetic parameters are considered to be intrinsic.

4.4. Effect of temperature

DBT hydrogenation was conducted at four different temperatures ranging from 120 to 210°*C* (other conditions at reference values). After the initial heating-up period (until the collection of the second sample), the temperature was kept constant as the reaction progressed. Concentration profiles for DBT and its hydrogenation products are given in Fig. 8, for each of these experiments. Experimental data shows fast DBT to H6-DBT conversion at higher temperatures, with nearly complete conversion within the first 100 *min* of the reaction. At 120°*C*, the reaction rate of this step is noticeably slower, but conversion over 95% is still achieved within the first 2 *h*. These results are expected, considering that both of the side benzene rings can hydrogenate in this reaction step. Preference of side rings is caused by steric hindrance and has been confirmed by Do et al. [30] for the temperature range of 120 to 210°*C* at 50 *bar*, over Ru/Al$_2$O$_3$ catalyst. Experimental profiles for H6-DBT change distinctly with temperature, which suggests a relatively strong temperature dependence of reaction rates for both the first and the second hydrogenation step. Finally, H18-DBT profiles have a similar experimental trend at all reaction temperatures, suggesting less prominent impact of temperature on the final hydrogenation step. Additionally, due to the side ring preference, significant formation of H18-DBT
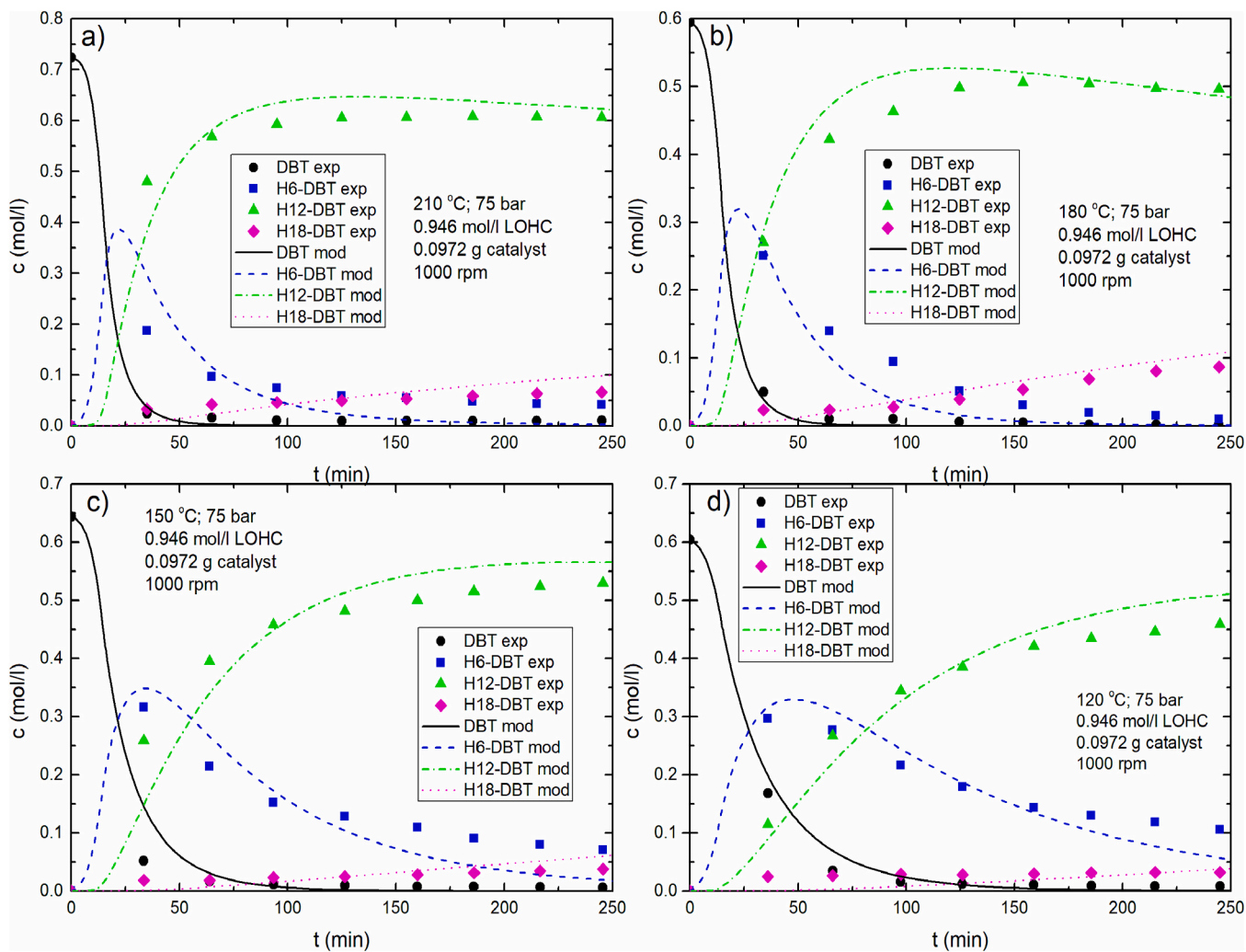
Fig. 8. DBT concentration profiles at: a) 210°C b) 180°C c) 150 °C d) 120 °C.
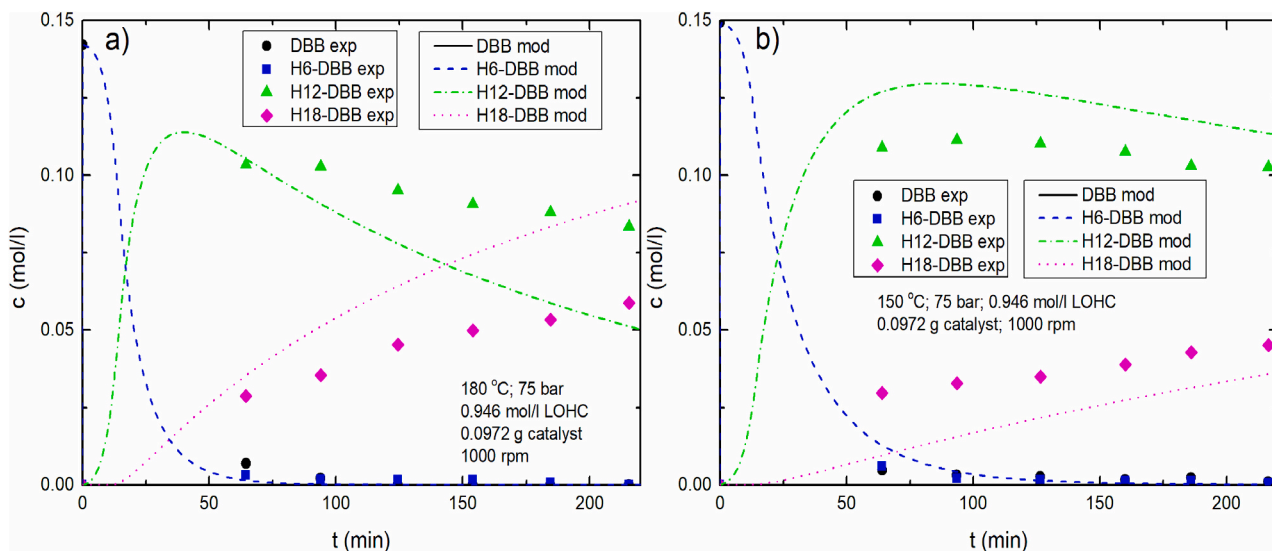

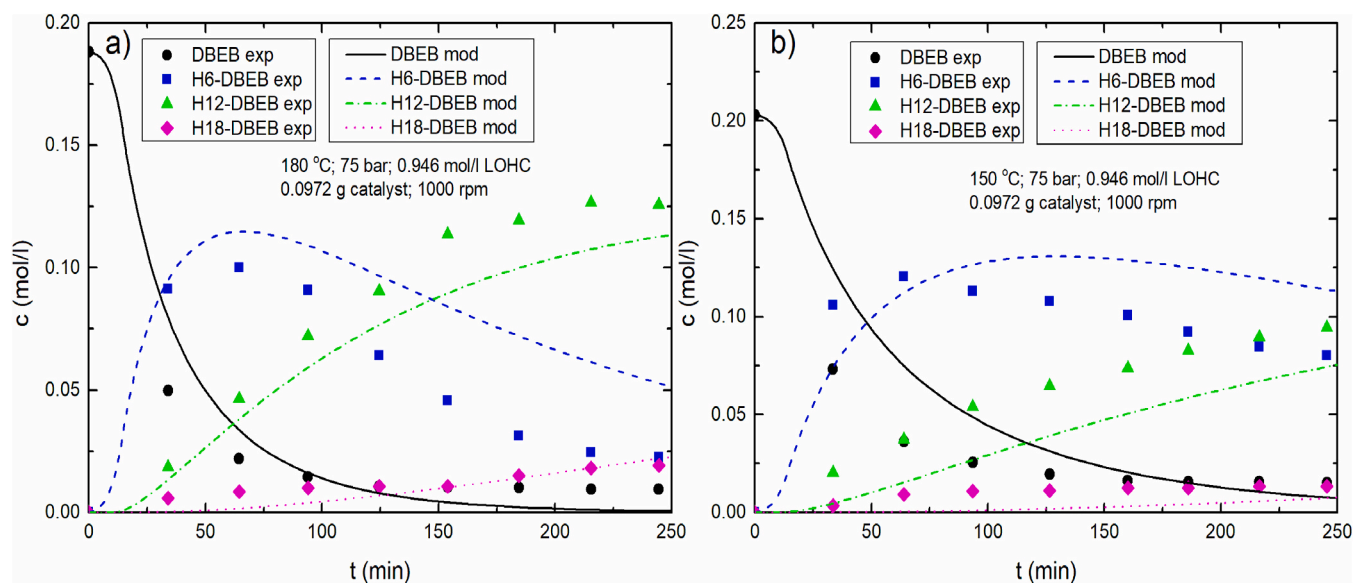**Fig. 9.** DBB concentration profiles at: a) 180°C b) 150 °C.

Fig. 10. DBEB profiles at 180°C (left) and 150 °C (right).

starts only after a substantial amount of H12-DBT has been formed, which is in accordance with literature [30]. Another interesting effect can be identified when looking at H18-DBT production for experiments at 180and 210°C. At 180°C, the achieved H18-DBT yield was 14.65%, whereas at 210°C H18-DBT yield reached only 9.12%. The decrease in H18-DBT production at 210°C can be explained by catalyst deactivation, confirmed by Jorschick et al. [47] for Ru-based catalyst at temperatures over 210°C. The value of H18-DBT yield also suggests that the temperature of 180°C is most suitable for DBT hydrogenation. Ali et al. [31] have reached a similar conclusion in their experimental study, where the optimal temperature for DBT hydrogenation in the presence of Raney-Ni catalyst was 170°C. The choice of catalyst for DBT hydrogenation will obviously have an impact on the optimal temperature value for this reaction.

Fig. 8 also illustrates model predictions for the influence of temperature on DBT hydrogenation. The model shows excellent agreement with the experimental trends, with slight deviations for H6-DBT concentrations, which may be the result of the quality of experimental data analysis. The estimated activation energies for the first and the second hydrogenation step are slightly higher than the activation energy for the last hydrogenation step, which corresponds well with the experimental trend of lowest temperature sensitivity for the final hydrogenation step, as seen in Fig. 8. The main difference in kinetic parameters can be observed for the pre-exponential factor of the last step, which was estimated to be three orders of magnitude lower than the values for the first two reaction steps.

Fig. 9 presents experimentally obtained results and predicted concentration profiles for DBB and all of its hydrogenation products at 150 and 180°C. Within the first hour of the reaction DBB conversion above 95% is reached for each reaction temperature. Moreover, <5% of the formed H6-DBB remains in the reaction mixture after the first 60 *min* for all temperatures except the lowest. Very subtle change in H6-DBT conversion with temperature illustrates slight temperature dependence of the reaction rates of the first two steps. Compared to DBT, DBB undergoes hydrogenation more easily since no additional functional groups can be found on the middle benzene ring (reduced steric hindrance). Thus, after 2 *h* of hydrogenation, only H12-DBB and H18-DBB
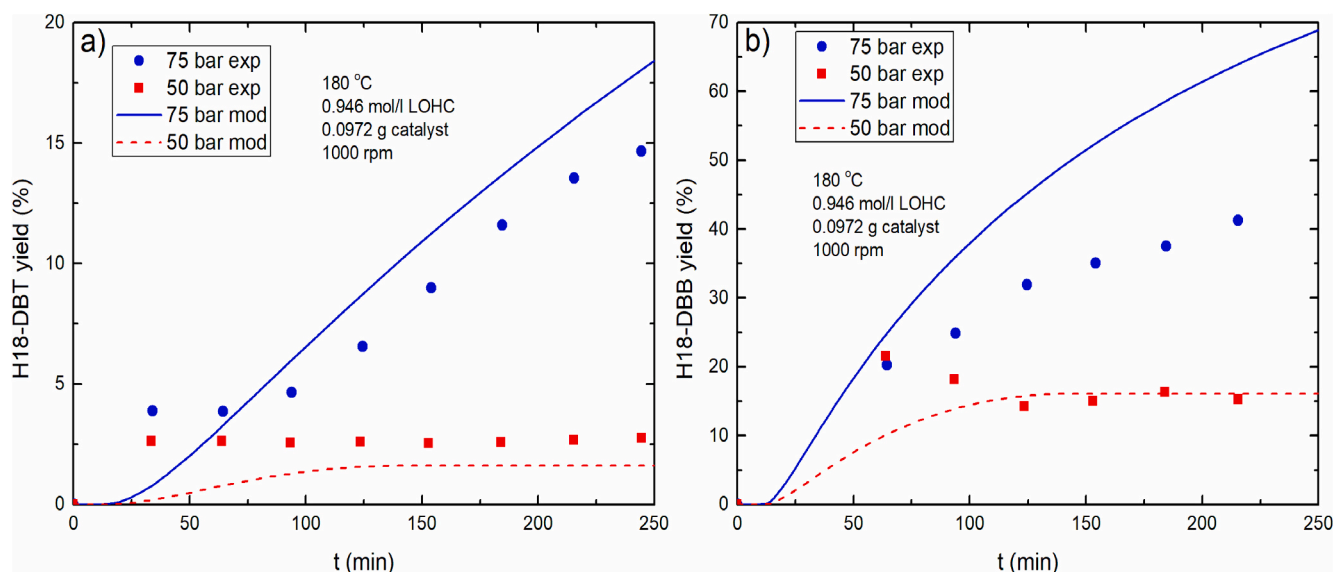

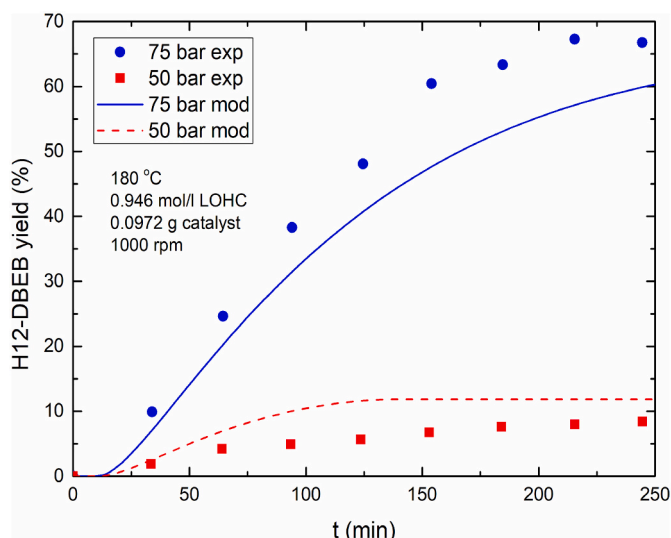**Fig. 11.** Pressure influence on: a) H18-DBT yield b) H18-DBB yield.

Fig. 12. Pressure influence on H12-DBEB yield.

can be found in the reaction mixture, as shown in Fig. 4. Experimental data for H12-DBB and H18-DBB concentrations suggest that the final hydrogenation step is slightly more sensitive to the reaction temperature than the previous two steps. The degree of total hydrogenation of DBB to H18-DBB is evidently much higher compared with DBT to H18-DBT hydrogenation. To illustrate, at $180°C$ the achieved H18-DBT yield after 3.5 *h* was 13.55%, whereas the production of H18-DBB reached a yield of 37.89%. These results indicate that DBB might be a better LOHC candidate than DBT, from the perspective of fast and complete hydrogenation. Nonetheless, further research regarding DBB stability, dehydrogenation conditions and kinetics are necessary to examine all potential limitations of DBB use for efficient hydrogen storage.

Experimentally identified fast hydrogenation of DBB to H12-DBB is well described by the model, which gives good predictions for DBB and H6-DBB conversions. Predicted concentration profiles for H12-DBB and H18-DBB follow a similar trend as the experimental data, but they deviate to a certain degree from the experimental points. This deviation is more prominent at higher temperatures, as seen from Fig. 9. This could be caused by the potential H18-DBB degradation, which has been

identified in the following experiments (section 4.5). In their research, Brückner et al. [17] have reported no significant by-product formation ($< 0.01\%$) within 72 *h* of H18-DBT dehydrogenation at $270°C$, in the presence of Pt/Al$_2$O$_3$ catalyst. However, Jorschick et al. [47] have reported methane formation during DBT hydrogenation over Ru/Al$_2$O$_3$ catalyst, for temperatures above $200°C$. Since most of the experiments in this study have been conducted at temperatures below $200°C$, potential DBT decomposition has been left out of the proposed model and the same was assumed for both DBB and DBEB. Nevertheless, the structural difference and the presence of the solvent could have led to some H18-DBB degradation in this study, which is not accounted for by the model. Since DBB accounts for only about 15% of the initial reaction mixture, the increase in model complexity was not deemed justifiable.

Influence of temperature on DBEB hydrogenation is displayed in Fig. 10, for experiments at 180and $150°C$. Experimental data shows that DBEB hydrogenates more slowly than DBT, which is probably due to the presence of an ethyl group in the molecule. For the experiment at $180°C$, experimental results show a decrease in H6-DBEB concentration due to significant H12-DBEB formation after the first 60 *min* of the reaction. The final value of the H12-DBEB yield at the end of the reaction was 66.75% for this experiment, while the final hydrogenation step yielded a small quantity of H18-DBEB (10.23% yield). For the reaction conducted at $150°C$, the reaction rate of the second step decreased noticeably, leading to the final H12-DBEB yield of only 46.50%. These results demonstrate that the second hydrogenation step is most sensitive to temperature. This has also been confirmed by the model, which predicts the highest activation energy for the second reaction step (32.01 *kJ/mol*). The model also agrees relatively well with the experimental trends for both DBEB and all of its products.

4.5. Effect of pressure

For the reactor system used in this study, the entire quantity of available hydrogen was introduced via pressurization at the beginning of the reaction. After a desired pressure was obtained, the heating-up process was initiated and this marked the beginning of the reaction. The initial hydrogen pressures implemented in this study were 50 and 75 *bar*, while additional experiments at 100 *bar* were conducted for model verification (section 4.9).

The influence of initial hydrogen pressure on H18-DBT and H18-DBB yields is presented in Fig. 11. The initial amount of hydrogen introduced
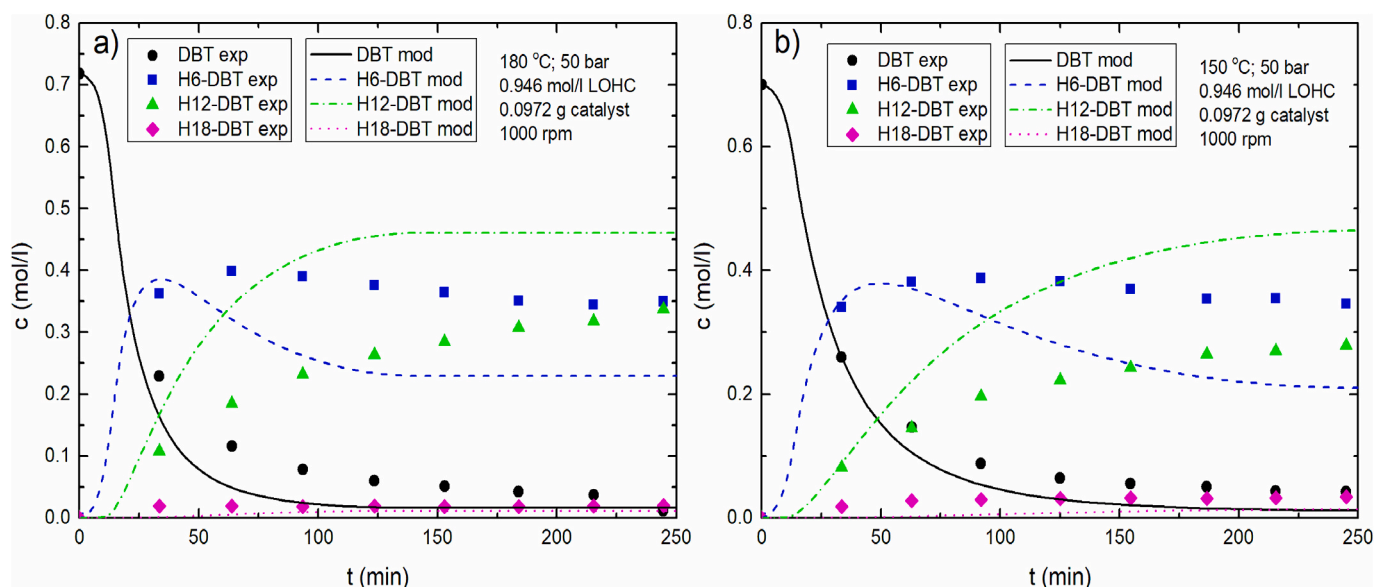

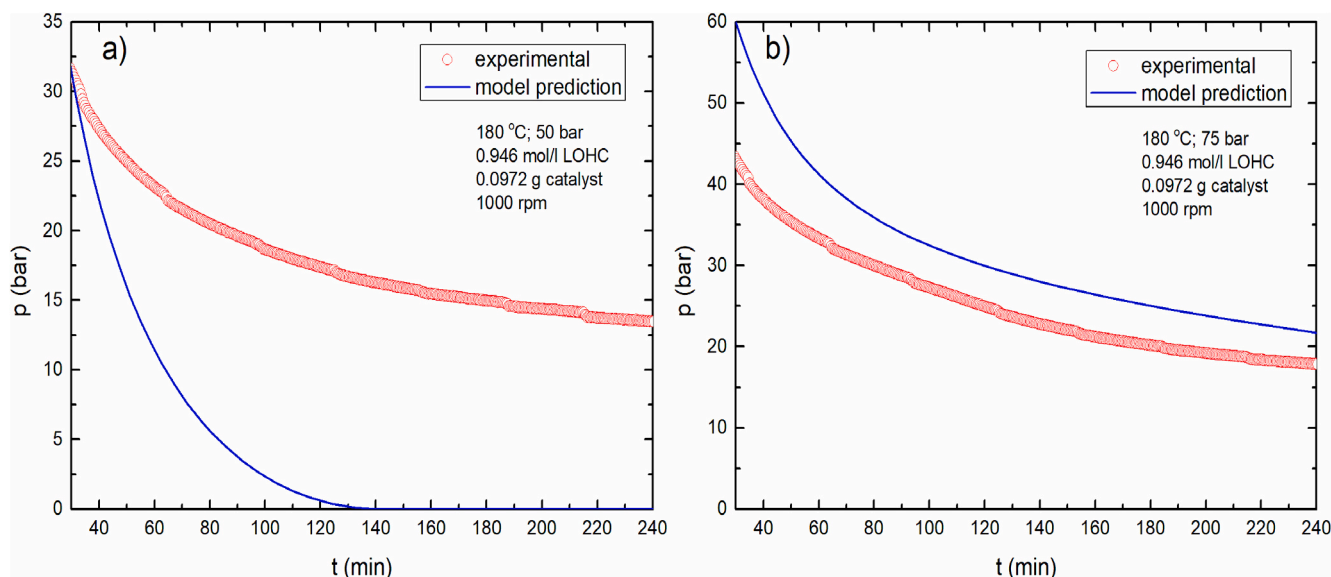**Fig. 13.** DBT concentration profiles at 50 bar and: a) 180°C b) 150 °C.

Fig. 14. Hydrogen pressure profiles for experiments at 180°C and: a) 50 bar b) 75 bar.
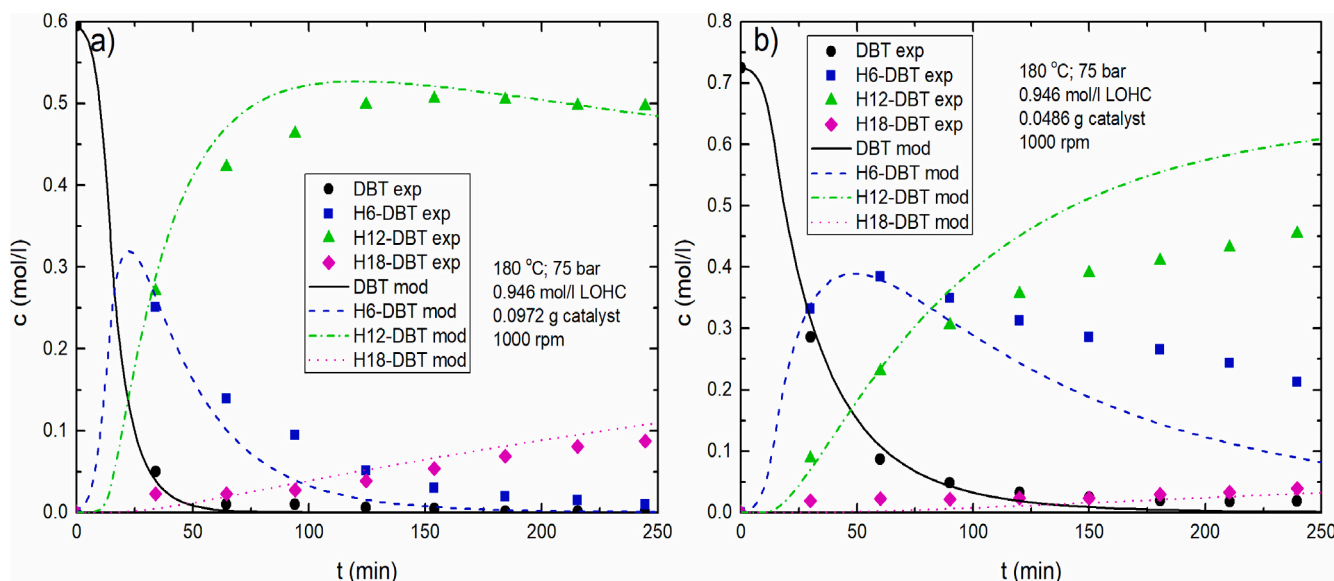

Fig. 15. Influence of catalyst amount on DBT concentration profiles for: a) 0.0972 g b) 0.0486 g.

at 75 bar was not sufficient for complete DBEB hydrogenation, so the pressure influence was illustrated with H12-DBEB yield profiles in Fig. 8. The initial pressure in the system dictates the amount of the limiting reactant (hydrogen) for the LOHC hydrogenation. Having that in mind, it is expected that higher pressure values will promote hydrogenation significantly, as shown in Figs. 11 and 12. H18-DBT and H12-DBEB yields at 50 *bar* hardly change after the first 90 *min* are almost constant, indicating that nearly all of the introduced hydrogen has reacted with LOHC molecules. H18-DBB profile at 50 *bar* (Fig. 11, right) has a distinctive maximum at about 60 *min*, which suggests that some decomposition processes reduce the quantity of H18-DBB present in the system, as the reaction progresses. It is safe to assume that H18-DBB dehydrogenation does not occur in this experiment due to the high reaction pressure (final pressure above 13 bar). As previously mentioned, DBB and its products could be more prone to by-product formation in the presence of Ru/Al₂O₃ catalyst compared to DBT, even at temperatures lower than 200°*C*.

Drastic changes in H18-DBT values are observed after the first 90 *min*

of the reaction, when H12-DBT concentration becomes substantial. After this point, H18-DBT yield increases almost linearly until the reaction is terminated. This indicates that relatively fast complete hydrogenation could be achieved with continuous hydrogen supply at pressures around 50 *bar*, which is also recommended in literature [17].

Based on the predicted concentration profiles, presented in Figs. 11 and 12, it can be observed that the model accurately predicts the trends for H18-DBT and H12-DBEB production, especially after the first hour of the reaction. The model deviation for H18-DBB yield are likely the result of the present H18-DBB decomposition, not described by the model, and simplified hydrogen solubility description, based on the solubility of this gas in n-hexane (solvent).

A set of experiments (# 5–8 in Table 2) was performed at lower initial pressure (50 *bar*) for four temperatures in the range of 120 to 210°*C*, to include both temperature and pressure influence. Fig. 13 gives concentration profiles for DBT and its hydrogenation products for experiments at 50 *bar* and temperatures of 180and 150°*C*. In these experiments, less hydrogen was available for the reaction, which led to
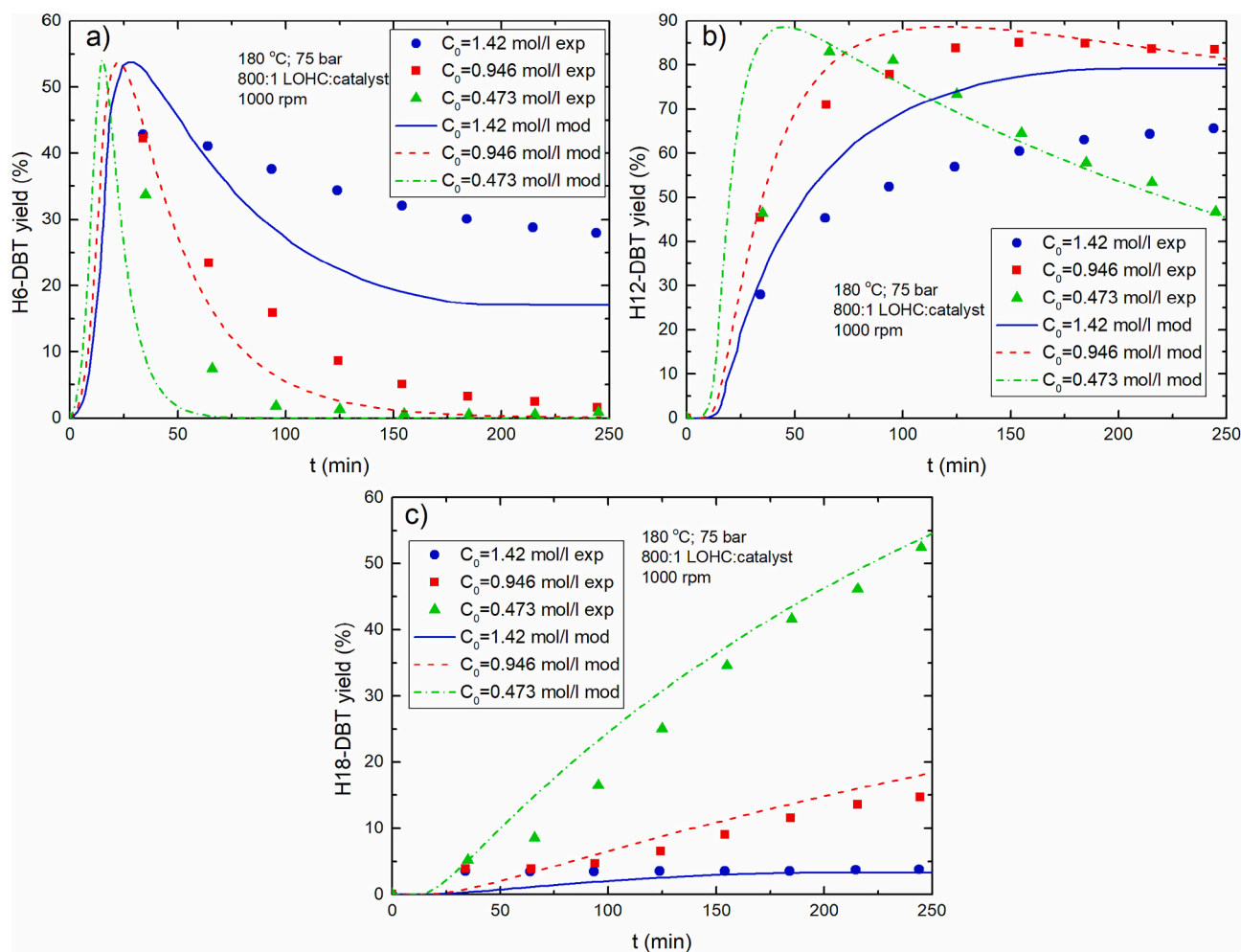
Fig. 16. Influence of the initial reactant concentration on: a) H6-DBT yield b) H12-DBT yield c) H18-DBT yield.

lower DBT conversions. At 150°C, DBT conversion after 4 h remained just under 95%. Despite the temperature variations, lower hydrogen pressure had a more pronounced influence on this reaction, since hydrogen was the limiting reactant. This is supported by the similar trends for H6-DBT and H12-DBT concentration profiles at two different temperatures, when the initial hydrogen pressure is reduced (compared to the reference value). Lastly, for both of these reactions, insufficient amount of hydrogen resulted in low H18-DBT production with yields under 5% for both presented temperatures.

At 50 *bar*, the quality of the predicted trends for these concentration profiles decreases with temperature increase. It is worth noting that in each experiment, the pressure in the system decreased as LOHC molecules hydrogenated, which lead to final pressures slightly above 10 *bar* for these experiments. Pressure reduction at higher temperature could have led to some solvent evaporation.

The possibility of solvent evaporation at low pressure and high temperature was further analyzed. Fig. 14 gives the comparison of measured and model-predicted hydrogen pressure in the system at 50 and 75 *bar* initial total pressure and 180°C. For the lower initial pressure, the model predicts complete hydrogen conversion and the pressure decrease to zero, although the measured pressure at the end of the reaction was 13.42 *bar*. In the case of solvent evaporation, the measured pressure should correspond to the partial pressure of n-hexane at the reaction conditions. Calculation of n-hexane partial pressure can be done using Raoult's law, with the vapor pressure obtained by using the Lee-Kesler equation (this procedure can be found in Supplementary material) [48]. The calculated vapor pressure at these conditions is

13.10 *bar*, while the partial pressure of n-hexane was found to be 11 *bar*. On the other hand, in case of the higher pressure, solvent evaporation is suppressed and the model gives significantly better predictions for hydrogen partial pressure (Fig. 14: right). These results strongly suggest that significant solvent evaporation occurs for the reactions at high temperatures and low initial hydrogen pressure.

4.6. Effect of the catalyst amount

The next reaction parameter, whose influence was investigated, was the amount of Ru/Al$_2$O$_3$ catalyst present in the system. Fig. 15 represents experimental results and model predictions for the reference experiment (Fig. 15: left) and the experiment with half of the reference catalyst amount (Fig. 15: right). Since the reaction occurs only at the available active sites of the catalyst, it was expected that the reduction of the catalyst amount would slow down all of the reaction steps. For the reference experiment, nearly complete DBT conversion is achieved within 2 h, whereas with the lower catalyst amount DBT conversion achieves 97.39% after 4 h. H6-DBT concentration profile has a more pronounced maximum when a larger amount of the catalyst is present and this peak is reached within the first hour of the reaction. At the end of the reaction with higher catalyst amount (0.0972 *g*) H6-DBT converts almost completely, leaving only H12-DBT and H18-DBT in the reaction mixture. For the experiment with lower amount (0.0486) of the catalyst, H6-DBT is still present after 4 h, with the yield of H18-DBT < 5.5%. These results prove that the reaction depends strongly on the number of available active sites, as expected. Additionally, for the experiment with
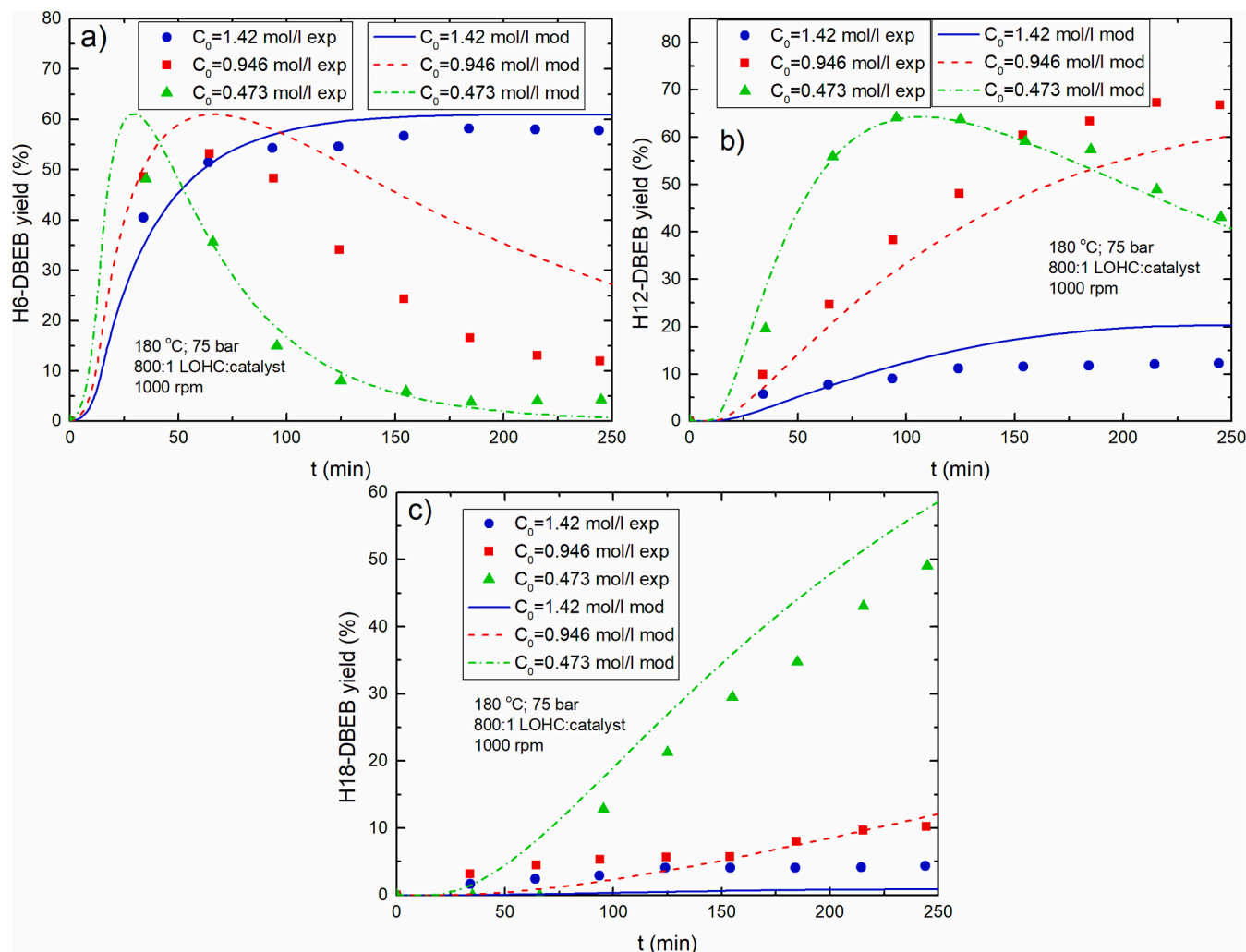
Fig. 17. Influence of the initial reactant concentration on: a) H6-DBEB yield b) H12-DBEB yield c) H18-DBEB yield.

less catalyst, 62.70% of H12-DBT is formed after 4 *h* of hydrogenation. Compared to that, the yield of H12-DBT obtained in the base case experiment reached 71% after just one hour, which promoted further hydrogenation and noticeable H18-DBT production.

Fig. 15 also presents the modeling results for these two experiments. The obtained fit follows the experimental trend well for the experiment with a smaller amount of catalyst. The model accurately predicts DBT conversion for this experiment, but slightly overestimates H6-DBT conversion in the second reaction step. This results in somewhat higher predictions for H12-DBT concentrations, compared to the experimentally obtained values. A possible reason for this deviation could be the difference in adsorption equilibrium constants for less and more hydrogenated molecules. In case of the reference experiment, DBT converts to H6-DBT almost completely within the first hour, while H6-DBT concentration decreases rapidly in the second hour of the reaction. Furthermore, quick DBT conversion is present in most of the conducted experiments. The results indicate that the estimated equilibrium constant actually better describes adsorption/desorption of H12-DBT and H18-DBT, than DBT and H6-DBT. That could also be the reason for some deviation in case of the experiment with a smaller catalyst amount, since H6-DBT is present in more significant concentrations.

4.7. Effect of the initial reactant concentration

Two experiments with varied initial LOHC concentration have been conducted and the obtained results compared to the base case experi-

ment, in attempts to identify the influence of this parameter. It is important to note that LOHC:catalyst ratio remained the same for each of these experiments. However, since the experiments were all performed at initial pressure of 75 *bar*, these experiments have different LOHC:hydrogen ratios. Fig. 16 displays yields for all DBT hydrogenation products, obtained in these three experiments. Decrease of the initial LOHC concentration promoted hydrogenation, because less hydrogen was needed for full LOHC hydrogenation, as hydrogen is the limiting reactant. For this experiment, a drastic decrease in H12-DBT yield can be observed, due to the significant H18-DBT production. These results indicate that improved continuous hydrogen supply could significantly promote the reaction even for higher initial LOHC concentrations.

The predicted concentration profiles follow the experimental trends relatively closely, especially in case of H18-DBT yield. For the lowest initial concentration, the model gives best quantitative predictions, which could again be explained by the large molar fraction of H12-DBT and H18-DBT in the mixture.

Influence of the initial LOHC concentration on yields of DBEB hydrogenation products is presented in Fig. 17. The obtained experimental trends for DBEB hydrogenation products have a similar trend to the corresponding DBT species, but with strong indication of slower hydrogenation in case of DBEB. This is most evident from the experiments with the highest initial LOHC concentration, where H6-DBEB does not decrease throughout the reaction, as is the case with H6-DBT (Fig. 16), while H12-DBT and H12-DBEB yields reach 65.70 and 12.27%, respectively. This is due to the fact that hydrogen is slightly more
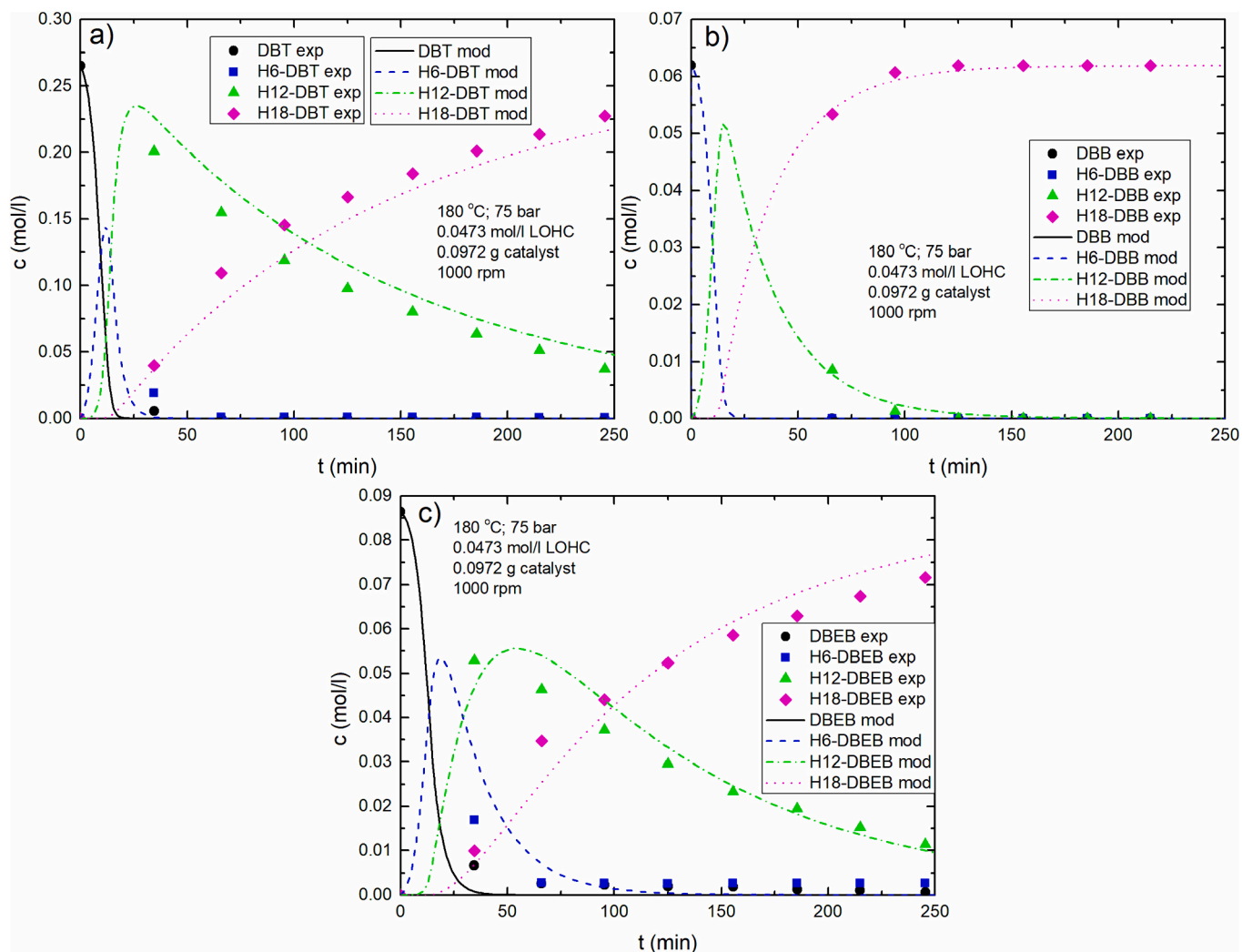
Fig. 18. Concentration profiles for experiment # 13 for: a) DBT b) DBB c) DBEB.
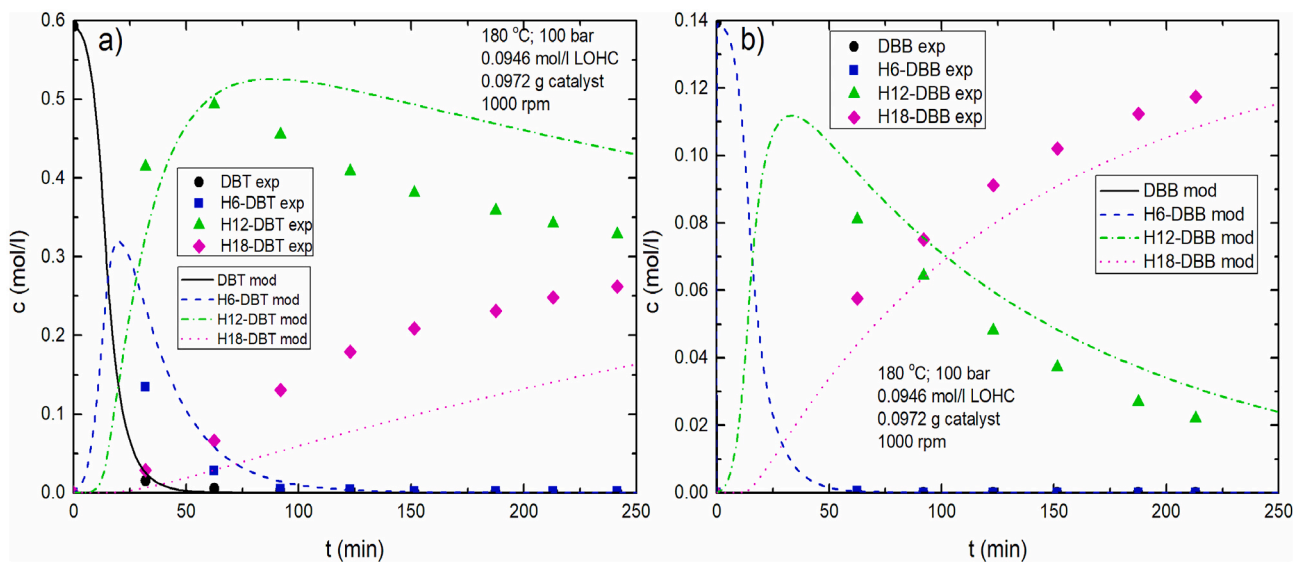

Fig. 19. Concentration profiles for experiments at 100 bar and 180°C for: a) DBT b) DBB.

selective towards DBT, compared to DBEB. However, when enough hydrogen is available for the reaction, as in the case of lowest initial LOHC concentration, the difference in achieved yields for DBT and DBEB products is smaller.

The predicted yields for DBEB products follow the experimentally obtained trends relatively well, as shown in Fig. 17. The quantitative imprecision of the predicted yield values could be contributed to the presence of the experimental error, as well as the fact that the model does not differentiate between hydrogenation products adsorption equilibrium constants.

4.8. Maximum hydrogenation experiments

Three experiments (#14–16 in Table 2) have been performed in attempts to achieve the highest possible hydrogenation degree of the initial LOHC. In these experiments, the lowest initial LOHC concentration of 0.473 *mol/l* was used (5 *ml* of LOHC). One of the experiments was conducted at the reference temperature and LOHC:catalyst ratio of 400(reference value: 800), i.e. 0.0972 *g* of Ru/Al$_2$O$_3$. The remaining two experiments were conducted at 210°*C*, with LOHC:catalyst ratio of 400and 800 (0.0972 and 0.0486 *g* of Ru/Al$_2$O$_3$, respectively). It is worth noting that industrial practice would promote hydrogenation by introducing larger quantities of hydrogen continuously, but this approach was not possible in laboratory conditions due to safety risks. Instead, hydrogenation has been promoted by decreasing the initial LOHC concentration and increasing the amount of the catalyst present in the system, at appropriate reaction temperatures.

Among selected, the highest degree of hydrogenation has been reached for the experiment at reference temperature, with the initial LOHC concentration of 0.473 *mol/l* and 0.0972 *g* of Ru/Al$_2$O$_3$ catalyst. The concentration profiles for all LOHC and their hydrogenation products for this experiment are given in Fig. 18. The obtained yields for H18-DBB, H18-DBT and H18-DBEB were 100%, 85.75% and 82.98%, respectively. Apart from the difference in the obtained yields for final hydrogenation products, it is important to notice that complete DBB conversion to H18-DBB occurs after only 2 *h* of the reaction, which is shorter than for other LOHC and again demonstrates easiest DBB hydrogenation.

The predicted concentration profiles, presented in Fig. 18, agree excellently with the experimental data for all organic species. This experiment has been conducted at reference initial pressure of 75 *bar*, which minimizes the model inaccuracy due to pressure influence (see section 4.5). Consistent with the previous discussion, the estimated values of equilibrium constants of LOHC molecules probably correspond better to the actual values for the higher hydrogenation products (H12-LOHC and H18-LOHC). In light of this, it can further be concluded that the quality of predictions for this model increases with the degree of LOHC hydrogenation.

4.9. Model verification at higher pressures

In order to determine the degree of pressure influence on model prediction quality versus the potential issue of equivalent equilibrium constants for LOHC hydrogenation products, three experiments (# 17–19 in Table 2) at 100 *bar* were kept for model verification (not included in parameter estimations). The first experiment was conducted at 100 *bar* and 180°*C*, with all other conditions at reference values. The next experiment was conducted at 150°*C*, while the only change in the last experiment was the increase of catalyst mass to 0.1945 *g* (LOHC: catalyst ratio of 400).

Fig. 19 shows the predicted concentration profiles for DBT (left) and DBB (right) and their hydrogenation products for the experiment at 100 *bar* and 180°*C*. In this experiment, LOHC hydrogenation has been promoted by introducing a larger amount of hydrogen (50% more hydrogen than in the reference experiment) in the reactor, which

resulted in very fast complete conversion of initial reactants to H12-DBT and H12-DBB. Nearly complete H6-DBT conversion is achieved after 1.5 *h*, whereas after just one hour, no DBB or H6-DBB has been detected in the reaction mixture. Based on the previous results, it has been concluded that the quality of model predictions increases with hydrogenation degree for experiments at the initial reaction pressure of 75 *bar* (see section 4.8). Since higher hydrogenation products are almost exclusively present in the experiment at 100 *bar*, the deviation of model predictions are more likely the result of the inaccurately described pressure influence (see section 4.5). However, the model still manages to give good predictions for concentration profile trends, with some deviations for DBT hydrogenation products.

5. Conclusions

The experimental part of this study explored the option of using DBB and DBEB as potential LOHC, alongside DBT. The results have shown that, despite slightly slower hydrogenation rates, DBEB could successfully be used as an LOHC. Reduced steric hindrance in case of DBB resulted in faster hydrogenation, compared to DBT. However, the use of DBB could be limited due to its low thermal stability, which is especially significant for the dehydrogenation process. This study also explored the influence of various experimental conditions, discovering that the optimal temperature in the presence of Ru/Al$_2$O$_3$ is 180°*C*. Due to safety measures, hydrogen was introduced through initial pressurization, making it the limiting reactant in most experiments. However, relatively high product yields obtained at 100 *bar* (44.22% of H18-DBT) after 4.5 *h* suggest that fast and complete hydrogenation could be achieved with continuous hydrogen supply at significantly lower pressures. The difference in DBT conversion for experiments at stirring speeds of 600 and 1000 *rpm* was <1%, which confirms that external mass transfer resistance becomes negligible for stirring speeds above 600 *rpm*.

The first microkinetic model for hydrogenation of DBT, DBB and DBEB in the presence of Ru/Al$_2$O$_3$, for different reaction temperature, pressure, initial reactant concentration and catalyst amount was successfully developed. The model gave very good prediction for concentration trends, confirming that this reaction can be described using the adopted Langmuir-Hinshelwood mechanism with dissociative hydrogen adsorption. Despite relatively high error values, the model gave accurate predictions of the temperature influence on each reaction step and the quality of the fit is notably better for the experiments with higher hydrogenation degree. The highest hydrogenation rates have been achieved for low initial LOHC concentration of 0.0473 *mol/l* and LOHC: catalyst ratio of 400, at 180°*C* and 75 *bar*. The achieved yields for the H18-DBB, H18-DBT and H18-DBEB were 100%, 85.75% and 82.98%, respectively, while the model predictions showed excellent agreement and the total RME was 17.46% for this experiment. Further development of the model would, aside from quantitative analysis improvement, require exploration of hydrogen solubility in the DBT-based mixtures and adsorption properties of the present LOHC molecules.

CRediT authorship contribution statement

Aleksandra Tomić: Writing – original draft, Methodology, Investigation. **Brett Pomeroy:** Writing – review & editing. **Branislav Todić:** Validation, Project administration, Data curation. **Blaž Likozar:** Resources, Funding acquisition. **Nikola Nikačević:** Supervision, Funding acquisition.

Declaration of competing interest

The authors declare that they have no known competing financial interests or personal relationships that could have appeared to influence the work reported in this paper.

Data availability

Data will be made available on request.

Acknowledgment

Appendix A. Supplementary data

Supplementary data to this article can be found online at https://doi.org/10.1016/j.apenergy.2024.123262.

References

[1] Rao PC, Yoon M. Potential Liquid-Organic Hydrogen Carrier (LOHC) systems: a review on recent progress. Energies 2020;13:6040. https://doi.org/10.3390/en13226040.

[2] 2030 Climate Target Plan. https://climate.ec.europa.eu/eu-action/european-green-deal/2030-climate-target-plan_en; 2023 (accessed May 15, 2023).

[3] Aakko-Saksa PT, Cook C, Kiviaho J, Repo T. Liquid organic hydrogen carriers for transportation and storing of renewable energy – review and discussion. J Power Sources 2018;396:803–23. https://doi.org/10.1016/j.jpowsour.2018.04.011.

[4] Niermann M, Timmerberg S, Drünert S, Kaltschmitt M. Liquid Organic Hydrogen Carriers and alternatives for international transport of renewable hydrogen. Renew Sustain Energy Rev 2021;135:110171. https://doi.org/10.1016/j.rser.2020.110171.

[5] Niermann M, Beckendorff A, Kaltschmitt M, Bonhoff K. Liquid Organic Hydrogen Carrier (LOHC) – assessment based on chemical and economic properties. Int J Hydrogen Energy 2019;44:6631–54. https://doi.org/10.1016/j.ijhydene.2019.01.199.

[6] Jang M, Jo YS, Lee WJ, Shin BS, Sohn H, Jeong H, et al. Reversible liquid organic hydrogen carrier: H2-release properties and an application to a fuel cell. ACS Sustain Chem Eng 2019;7:1185–94. https://doi.org/10.1021/acssuschemeng.8b04835.

[7] Niermann M, Drünert S, Kaltschmitt M, Bonhoff K. Liquid organic hydrogen carriers (LOHCs) – techno-economic analysis of LOHCs in a defined process chain. Energ Environ Sci 2019;12:290–307. https://doi.org/10.1039/C8EE02700E.

[8] Brigljević B, Byun M, Lim H. Design, economic evaluation, and market uncertainty analysis of LOHC-based, CO2 free, hydrogen delivery systems. Appl Energy 2020;274:115314. https://doi.org/10.1016/j.apenergy.2020.115314.

[9] Bourane A, Elanany M, Pham TV, Katikaneni SP. An overview of organic liquid phase hydrogen carriers. Int J Hydrogen Energy 2016;41:23075–91. https://doi.org/10.1016/j.ijhydene.2016.07.167.

[10] Jorschick H, Vogl M, Preuster P, Bösmann A, Wasserscheid P. Hydrogenation of liquid organic hydrogen carrier systems using multicomponent gas mixtures. Int J Hydrogen Energy 2019;44:31172–82. https://doi.org/10.1016/j.ijhydene.2019.10.018.

[11] Yang C, Ogden J. Determining the lowest-cost hydrogen delivery mode. Int J Hydrogen Energy 2007;32:268–86. https://doi.org/10.1016/j.ijhydene.2006.05.009.

[12] Müller K. Technologies for the storage of hydrogen Part 1: Hydrogen storage in the narrower sense. ChemBioEng Rev 2019;6:72–80. https://doi.org/10.1002/cben.201900009.

[13] Wang C, Astruc D. Recent developments of nanocatalyzed liquid-phase hydrogen generation. Chem Soc Rev 2021;50:3437–84. https://doi.org/10.1039/D0CS00515K.

[14] Hurskainen M, Ihonen J. Techno-economic feasibility of road transport of hydrogen using liquid organic hydrogen carriers. Int J Hydrogen Energy 2020;45:32098–112. https://doi.org/10.1016/j.ijhydene.2020.08.186.

[15] Wunsch A, Mohr M, Pfeifer P. Intensified LOHC-dehydrogenation using multi-stage microstructures and Pd-based membranes. Membranes 2018;8:112. https://doi.org/10.3390/membranes8040112.

[16] Andersson J, Grönkvist S. Large-scale storage of hydrogen. Int J Hydrogen Energy 2019;44:11901–19. https://doi.org/10.1016/j.ijhydene.2019.03.063.

[17] Brückner N, Obesser K, Bösmann A, Teichmann D, Arlt W, Dungs J, et al. Evaluation of industrially applied heat-transfer fluids as liquid organic hydrogen carrier systems. ChemSusChem 2014;7:229–35. https://doi.org/10.1002/cssc.201300426.

[18] Modisha P, Gqogqa P, Garidzirai R, Ouma CNM, Bessarabov D. Evaluation of catalyst activity for release of hydrogen from liquid organic hydrogen carriers. Int J Hydrogen Energy 2019;44:21926–35. https://doi.org/10.1016/j.ijhydene.2019.06.212.

[19] Ouma CNM, Modisha PM, Bessarabov D. Catalytic dehydrogenation onset of liquid organic hydrogen carrier, perhydro-dibenzyltoluene: the effect of Pd and Pt subsurface configurations. Comput Mater Sci 2020;172:109332. https://doi.org/10.1016/j.commatsci.2019.109332.

[20] Lee S, Lee J, Kim T, Han G, Lee J, Lee K, et al. Pt/CeO2 catalyst synthesized by combustion method for dehydrogenation of perhydro-dibenzyltoluene as liquid organic hydrogen carrier: effect of pore size and metal dispersion. Int J Hydrogen Energy 2021;46:5520–9. https://doi.org/10.1016/j.ijhydene.2020.11.038.

[21] Solymosi T, Auer F, Dürr S, Preuster P, Wasserscheid P. Catalytically activated stainless steel plates for the dehydrogenation of perhydro dibenzyltoluene. Int J Hydrogen Energy 2021;46:34797–806. https://doi.org/10.1016/j.ijhydene.2021.08.040.

[22] Kim CH, Lee M-W, Jang JS, Lee SH, Lee K-Y. Enhanced activity of a WOx-incorporated Pt/Al2O3 catalyst for the dehydrogenation of homocyclic LOHCs: effects of impregnation sequence on Pt–WOx interactions. Fuel 2022;313:122654. https://doi.org/10.1016/j.fuel.2021.122654.

[23] Shi L, Zhou Y, Tan X, Qi S, Smith KJ, Yi C, et al. Dielectric barrier discharge plasma grafting carboxylate groups on Pt/Al2O3 catalysts for highly efficient hydrogen release from perhydro-dibenzyltoluene. Cat Sci Technol 2022;12:1441–9. https://doi.org/10.1039/D1CY01652K.

[24] Zhou J, Chung JS, Kang SG. Designing Pt-based subsurface alloy catalysts for the dehydrogenation of perhydro-dibenzyltoluene: a first-principles study. Appl Surf Sci 2022;579:152142. https://doi.org/10.1016/j.apsusc.2021.152142.

[25] Peters R, Deja R, Fang Q, Nguyen VN, Preuster P, Blum L, et al. A solid oxide fuel cell operating on liquid organic hydrogen carrier-based hydrogen – a kinetic model of the hydrogen release unit and system performance. Int J Hydrogen Energy 2019;44:13794–806. https://doi.org/10.1016/j.ijhydene.2019.03.220.

[26] Geiling J, Steinberger M, Ortner F, Seyfried R, Nuß A, Uhrig F, et al. Combined dynamic operation of PEM fuel cell and continuous dehydrogenation of perhydro-dibenzyltoluene. Int J Hydrogen Energy 2021;46:35662–77. https://doi.org/10.1016/j.ijhydene.2021.08.034.

[27] Lee S, Han G, Kim T, Yoo Y-S, Jeon S-Y, Bae J. Connected evaluation of polymer electrolyte membrane fuel cell with dehydrogenation reactor of liquid organic hydrogen carrier. Int J Hydrogen Energy 2020;45:13398–405. https://doi.org/10.1016/j.ijhydene.2020.02.129.

[28] Bulgarin A, Jorschick H, Preuster P, Bösmann A, Wasserscheid P. Purity of hydrogen released from the Liquid Organic Hydrogen Carrier compound perhydro dibenzyltoluene by catalytic dehydrogenation. Int J Hydrogen Energy 2020;45:712–20. https://doi.org/10.1016/j.ijhydene.2019.10.067.

[29] Ali A, Rohini AK, Lee HJ. Dehydrogenation of perhydro-dibenzyltoluene for hydrogen production in a microchannel reactor. Int J Hydrogen Energy 2022;47:20905–14. https://doi.org/10.1016/j.ijhydene.2022.04.212.

[30] Do G, Preuster P, Aslam R, Bösmann A, Müller K, Arlt W, et al. Hydrogenation of the liquid organic hydrogen carrier compound dibenzyltoluene – reaction pathway determination by 1H NMR spectroscopy. React Chem Eng 2016;1:313–20. https://doi.org/10.1039/C5RE00080G.

[31] Ali A, Udaya Kumar G, Lee HJ. Parametric study of the hydrogenation of dibenzyltoluene and its dehydrogenation performance as a liquid organic hydrogen carrier. J Mech Sci Technol 2020;34:3069–77. https://doi.org/10.1007/s12206-020-0638-x.

[32] Ali A, Kumar GU, Lee HJ. Investigation of hydrogenation of dibenzyltoluene as liquid organic hydrogen carrier. Mater Today: Proc 2021;45:1123–7. https://doi.org/10.1016/j.matpr.2020.03.232.

[33] Kim TW, Kim M, Kim SK, Choi YN, Jung M, Oh H, et al. Remarkably fast low-temperature hydrogen storage into aromatic benzyltoluenes over MgO-supported Ru nanoparticles with homolytic and heterolytic H2 adsorption. Appl Catal Environ 2021;286:119889. https://doi.org/10.1016/j.apcatb.2021.119889.

[34] Kim TW, Jeong H, Jo Y, Kim D, Park JH, Kim SK, et al. Advanced heterolytic H2 adsorption of K-added Ru/MgO catalysts for accelerating hydrogen storage into aromatic benzyltoluenes. J Energy Chem 2022;71:333–43. https://doi.org/10.1016/j.jechem.2022.03.047.

[35] Aslam R, Khan MH, Ishaq M, Müller K. Thermophysical studies of dibenzyltoluene and its partially and fully hydrogenated derivatives. J Chem Eng Data 2018;63:4580–7. https://doi.org/10.1021/acs.jced.8b00652.

[36] Geburtig D, Preuster P, Bösmann A, Müller K, Wasserscheid P. Chemical utilization of hydrogen from fluctuating energy sources – catalytic transfer hydrogenation from charged liquid organic hydrogen carrier systems. Int J Hydrogen Energy 2016;41:1010–7. https://doi.org/10.1016/j.ijhydene.2015.10.013.

[37] Dürr S, Müller M, Jorschick H, Helmin M, Bösmann A, Palkovits R, et al. Carbon dioxide-free hydrogen production with integrated hydrogen separation and storage. ChemSusChem 2017;10:42–7. https://doi.org/10.1002/cssc.201600435.

[38] Jorschick H, Preuster P, Dürr S, Seidel A, Müller K, Bösmann A, et al. Hydrogen storage using a hot pressure swing reactor. Energ Environ Sci 2017;10:1652–9. https://doi.org/10.1039/C7EE00476A.

[39] Sotoodeh F, Smith KJ. Kinetics of hydrogen uptake and release from heteroaromatic compounds for hydrogen storage. Ind Eng Chem Res 2010;49:1018–26. https://doi.org/10.1021/ie9007002.

[40] Knutti R, Bühler RE. Kinetics of the hydrogen atom reactions with benzene, cyclohexadiene and cyclohexene: hydrogenation mechanism and ring cleavage. Chem Phys 1975;7:229–43. https://doi.org/10.1016/0301-0104(75)87005-4.

[41] Kabadi VN. Improvement of hydrogen solubility and entrainment in hydrocracker feedstocks. Final technical report, North Carolina Agricultural and Technical State Univ., Greensboro, NC (United States). Dept. of Chemical Engineering; 1997. https://doi.org/10.2172/515515.

[42] Kim H, Park N-K, Lee T, Um M-H, Kang M. Preparation of nanosized α - Al 2 O 3 particles using a microwave pretreatment at mild temperature. Adv Mater Sci Eng 2012;2012. https://doi.org/10.1155/2012/920105.

[43] Bełtowska-Lehman E, Góral A, Indyka P. Electrodeposition and characterization of Ni/Al2O3 nanocomposite coatings, archives of metallurgy and materials; 2011; no 4 December. https://journals.pan.pl/dlibra/publication/99622/edition/85923; 2011.

[44] O'Connell K, Regalbuto JR. High sensitivity silicon slit detectors for 1 nm powder XRD size detection limit. Catal Lett 2015;3:777–83. https://doi.org/10.1007/s10562-015-1479-6.

[45] Li D, Li R, Lu M, Lin X, Zhan Y, Jiang L. Carbon dioxide reforming of methane over Ru catalysts supported on Mg-Al oxides: a highly dispersed and stable Ru/Mg(Al)O catalyst. Appl Catal Environ 2017;200:566–77. https://doi.org/10.1016/j.apcatb.2016.07.050.

[46] Liu Y, Huang F-Y, Li J-M, Weng W-Z, Luo C-R, Wang M-L, et al. In situ Raman study on the partial oxidation of methane to synthesis gas over Rh/Al2O3 and Ru/Al2O3 catalysts. J Catal 2008;256:192–203. https://doi.org/10.1016/j.jcat.2008.03.009.

[47] Jorschick H, Bulgarin A, Alletsee L, Preuster P, Bösmann A, Wasserscheid P. Charging a liquid organic hydrogen carrier with wet hydrogen from electrolysis. ACS Sustain Chem Eng 2019;7:4186–94. https://doi.org/10.1021/acssuschemeng.8b05778.

[48] Lee BI, Kesler MG. A generalized thermodynamic correlation based on three-parameter corresponding states. AIChE J 1975;21:510–27. https://doi.org/10.1002/aic.690210313.